

1 Anonymous Referee #1
2 Received and published: 30 August 2018

3
4 **Author Responses in red.**

5
6 **General Remarks**

7 The study by McGrath et al. addresses the question of the temporal stability of patterns
8 of snow accumulation on mountain glaciers. To my opinion, this is an excellently and
9 clearly written study. The authors use a very comprehensive dataset, spanning five
10 years and two glaciers. Furthermore, they provide insight on the implications of their
11 findings for glacier mass balance measurements using the glaciological method.
12 As a general recommendation, I suggest that the authors provide an only slightly more
13 detailed but more systematic overview to (i) the characteristics of the two glaciers and
14 (ii) the measurements that have been carried out there 1966-2009 and 2009 to present.
15 Furthermore, I believe that the last paragraph in Section 5.3 “Winter mass balance
16 comparisons” warrants a few more details. It appears interesting that detailed measurements
17 of winter mass balance seem to be able to reduce the agreement between
18 geodetic and glaciological measurements. However, I believe clarity of the argumentation
19 could benefit from adding a few more details.

20
21 **Detailed Remarks**

22 Lines 136: The reader does not know at which elevation the glacier is located. Hence,
23 provide a reference (e.g. is this at the ELA, below the glacier tongue or at the top?).
24 Only Figs. S3 and S4 would provide this information, but I recommend introducing the
25 glaciers in a bit more detailed manner (e.g. max and min elevation, typical ELA).
26 **We have added additional details regarding the elevation range and median ELA for both**
27 **glaciers.**

28
29 Line 139: Maybe better “lower” instead of “low”, this is still a respectable amount of
30 precipitation for many glaciers elsewhere.
31 **Good point, we have changed to less.**

32
33 Section 3.2: There are no snow probings in the accumulation zone? I fully understand
34 that you do not apply probing in the accumulation area, but ask myself here whether
35 there are any data from the accumulation area. Are the four locations where you dug
36 snow pits located in the accumulation zone? Or some of them in the accumulation
37 zone? I understand that they are visible on the plots but there is no information on the
38 typical elevation of the ELA.
39 **No, we do not probe in the accumulation zone because of the uncertainty in identifying the**
40 **summer surface where the seasonal snow is underlain by firm. Typically two of our pit/core**
41 **locations on each glacier are in the accumulation zone. We have clarified this in the manuscript.**

42
43 Lines 93: Just curious, why the irregular sampling interval?

44 **We use a regular sampling interval in the snowpit portion, but use natural breaks in the core to**
45 **partially define the sampling interval. We have clarified the wording of this sentence in the**
46 **manuscript.**

47
48 Line 227: Maybe you could add a brief explanation of Sb. The following sentence is
49 not clear to me. In particular, it is not fully clear to me whether lines 228 to 231 explain
50 Sb or explain how it is calculated.

51 We have added a brief explanation of Sb and explicitly refer the reader to the Winstral et al.
52 (2002) reference for further details.
53
54 Section 3.5: This section is, to my opinion, not fully concise. It appears to me that the
55 history of the measurements is insufficiently described. For example you mention that
56 the measurements were sparse, but only later you write of a three-stake network. Have
57 there been only three stakes 1966 to 2009, i.e. "sparse" refers to three measurements?
58 We have added additional details to Section 3.5 to clarify the history of the stake networks.
59
60 Line 338: Remove second dot.
61 Done.
62
63 Lines 358: The gradients are a function of time. Maybe mention somewhere that they
64 refer to the accumulation season.
65 Done.
66
67 Lines 587 to 589: True, but it might also be worth mentioning that glaciers preferably
68 form where more snow accumulates than on average (e.g. Kotlyakov and Krenke,
69 1982). The smaller the glacier, the stronger this effect. Hence, while snow measurements
70 on a glacier do minimize the risk of errors due to small scale effects, they might
71 increase the risk of a systematic positive bias.
72 Good point. We have modified how we present this idea to acknowledge this potential bias.
73
74 Line 596: Sounds almost a bit as if the data gaps are not safe to access on ground
75 surveys :-). Maybe rearrange?
76 We have clarified this sentence.
77
78 Line 600: Not sure, should there be a hyphen: "under-sampled"?
79 Corrected.
80
81 Lines 639-654: This paragraph makes a very interesting point. I believe it is worth
82 providing a few more details (see suggestions below).
83 Thanks. Please see responses below.
84
85 Line 641: This is somewhat difficult to understand, what do you mean with "stake
86 solution"? Do you mean average annual (or winter?) mass balance calculated from the
87 stake measurements? Over which time period?
88 We have clarified the terminology and the time scales in the manuscript.
89
90 Line 642: Unclear what is meant with -0.43 m w.e. a-1. Do you have to subtract 0.43 m
91 w.e. from annual glaciological mass balance ("stake solution") to achieve a decadal
92 mass balance in agreement with geodetic surveys?
93 Yes, for Wolverine Glacier, we subtract 0.43 m w.e. a⁻¹ from the glaciological mass balance time-
94 series to align it with the geodetic solution.
95
96 Line 646: -1 m w.e. a-1 sounds quite extreme but is difficult to assess without more
97 detailed insight into (i) how you interpolated annual mass balance based on the stake
98 measurements, and (ii) over which time period you compare geodetic and glaciological
99 mass balance. If I understand your interpretation correctly, it might be possible that
100 the stake network captures winter accumulation reasonably well (and it appears likely
101 that GPR surveys do this even better) while at the same time the stake network is not

102 representative for measuring summer ablation?
103 Yes, the -1 m w.e. a^{-1} is quite large. The details of the spatial interpolations and geodetic
104 calibrations have been previously published (van Beusekom et al., 2010 and O'Neel et al., 2014)
105 and are referenced in Section 3.5. We feel that it is outside the scope of the current paper to
106 present these details here as that is not the focus of the work. Our interpretation is that the stakes
107 are underestimating winter accumulation (especially with the limited number of stakes and site-
108 index approach for extrapolating), and therefore must really be missing ablation elsewhere on the
109 glacier.
110
111 Line 873-875: This paper appears not to be cited in the main text. Remove from
112 references or add citation.
113 Good catch. We've added this citation in where we previously intended.
114
115 References
116 Kotlyakov, V. M. & Krenke, A. N. (1982): Investigations of the hydrological conditions
117 of alpine regions by glaciological methods, Symposium at Exeter 1982 – Hydrological
118 aspects of alpine and high mountain areas, IAHS Press: Wallingford, 138, 31-42.
119
120
121 M. Pelto (Referee)
122 mauri.pelto@nichols.edu
123 Received and published: 19 September 2018
124 McGrath et al (2018) provide a detailed comparison of GPR accumulation measurements
125 and in situ observations on two Alaskan glaciers where long term glacier mass
126 balance monitoring has also occurred. To fill in areas lacking observations they used
127 two statistical approaches. They further explored six different approaches to estimating
128 glacier wide mass balance. Overall this paper has considerable value: 1) For identifying
129 the potential for GPR to validate reference stake observations on glaciers with
130 ongoing mass balance observations. 2) In assessment of inter annual variability of the
131 winter accumulation pattern and 3) In best practices for filling in data gaps.
132
133 The suggested revisions almost all fall into the category of additional references that
134 either support their observations and or provide an avenue for a more robust comparison
135 and contrast with other studies and methods. The authors underestimate the
136 number of studies that have used detailed in situ winter balance observations and detailed
137 in situ mass balance observations that can be used to address the question of
138 inter-annual spatial variability of winter accumulation in SWE.
139 Thanks for these suggestions. We have added additional details to the introduction
140 acknowledging this category of work that we hadn't previously considered in this context.
141
142 Specific Comments:
143 15: “: : observations on two glaciers in Alaska during the spring for five consecutive
144 years.
145 Done.
146
147 34: “: : of winter accumulation in SWE is only a : : :”
148 Done.
149
150 51: Many alpine glaciers have much a higher density of measurements in the spring
151 via probing than late summer using only stakes note the NVE network in Norway for
152 example, this should be acknowledged.

153 We have acknowledged these extensive probing datasets in the introduction.
154
155 93: It is true in the context of snow distribution on glaciers that inter-annual variability
156 has not been examined a great deal, however, a number of studies have examined
157 this in terms of annual mass balance and specific observations of winter and summer
158 balance at specific points note Vincent et al (2017). Could be worth citing Fountain and
159 Vecchia (1999) who look at how many stakes are needed for annual balance work, but
160 this does have bearing on winter balance. There are also numerous detailed published
161 multi-year winter balance maps that have been used by investigators to identify that
162 in fact there is limited inter-annual variability on their particular glacier justifying the
163 use of stakes in their processes, such as on Silvretta, Hinterisferner, Nigardsbreen,
164 Storbreen, Storgalcaren, White, Urumqi etc.
165 We have included references to these extensive snow probe datasets that are collected as part of
166 various glacier monitoring programs. We appreciate the suggestions re: annual mass balance, and
167 have added a sentence noting this “time-stability” in the spatial pattern of annual balances.
168 However, we’re hesitant to develop this point further, as we feel it is most appropriate to keep the
169 introduction focused on previous work that specifically examines winter mass balance.
170
171 114: This assumption can be verified in other ways for annual balance, for example
172 the WGMS reports the relationship between snowline and annual balance or ELA and
173 annual balance for all glaciers in the detailed reports of their bulletin. If the correlation
174 is good that indicates the consistency of the annual balance distribution and cannot be
175 achieved without a consistent SWE distribution (WGMS, 2017). Rabatel et al (2017)
176 conclude that, “the snow-map method shows better performance for the quantification
177 of the winter SMB because the method is based on the variations of the seasonal altitude
178 of the snow cover distribution, which are significantly representative of the winter
179 SMB; whereas in summer, the variations of the seasonal altitude of the snow cover
180 distribution are lower and limited to representing the high year-to-year variations of
181 summer SMB.” The approach of this study identifies limited inter-annual variability and
182 uses a separate approach.
183 This is a great suggestion for an additional approach to further investigate/corroborate the results
184 presented here, but consider it to be outside the scope of the current manuscript.
185
186 139: Any temperature gradient information that can be reported?
187 Although temperature gradient observations do exist at these glaciers for limited temporal
188 periods, we feel that these observations would not contribute to the analyses presented here and
189 would require a significant amount of text to introduce and fully explain.
190
191 200: A mean density was found to be most representative on the Greenland Ice Sheet
192 as well, would be useful to reference (Fausto et al, 2018).
193 We have added this reference to the manuscript.
194
195 362: Worth noting other balance gradients, can be done in discussion at line 532
196 instead of at this specific location. Lemon Creek= 470 mm 100 m-1 (Pelto et al, 2013)
197 Taku Glacier= 350 mm 100 m-1 (Pelto, 2008). What about on Eluktna and Scott Glacier
198 (McGrath et al, 2015)?
199 We have added this point and associated references in the Discussion.
200
201 387: Exceeded by how much?
202 This difference was variable from year to year, so we have decided not to state these values in the
203 text and instead refer the reader to Figure S2 where these differences can be observed.

204
205 387:”: : in the northeast quadrant of the glacier where wind drifting is prevalent.”
206 Added.
207
208 421: This variability from scour to deposition zones illustrates the importance of stake
209 placement in such a portion of the glacier that is neither scour nor deposition.
210 This is discussed in Section 5.3.1. in further detail.
211
212 447: Figure 12 add little value.
213 We don’t fully understand what this comment is specifically referring to however, the value
214 reported in this sentence is derived from Figure 12 and thus we feel it is appropriate to cite it in
215 this location.
216
217 481: Is this typically expected to be the case? It seems not so what is typical for this
218 stake location?
219 No, this is not what was expected and we explore this discrepancy in Section 5.3.
220
221 517: For many glaciers the transient snow line is a single distinct feature from early
222 until late summer. This indicates the similarity of accumulation along that line across
223 the width of the glacier in that elevation range (Mernild et al 2013). Is this the case on
224 Wolverine or Gulkana Glacier early in the summer season? The images I have seen
225 of the TSL on Wolverine indicate this to be the case note Figure 2 from McGrath et al
226 (2015).
227 The TSL on Wolverine and Gulkana is typically not a single distinct feature through the summer.
228 This is an example of where the GPR observations really help to illustrate the spatiotemporal
229 variability in accumulation patterns.
230
231 549: Lemon Creek Glacier also has wind scour leading to less accumulation at the
232 very highest elevations as at least one of your authors has observed.
233 We have added a sentence noting this point, but are not aware of an available citation.
234
235 564: Do your result allow determination if the redistribution represents any net change
236 in accumulated SWE or simply increasing the variability is SWE distribution?
237 No, our results do not allow us to determine this point as we don’t have sufficient off-glacier
238 observations to quantify SWE in these locations and thus relative changes in SWE through
239 redistribution.
240
241 637: Illustrates issues of a small network on glaciers with different accumulation basins.
242 We have added a sentence to address this point.
243
244 643: I am confused that Fig. 13 shows a negative bias, what am I missing?
245 In Figure 13, we are comparing the glaciological (stake) B_w estimates to the GPR derived B_w
246 estimates, which shows that the glaciological estimates are negatively biased. In this paragraph,
247 we are discussing the geodetic-glaciological correction, and how the GPR results suggest that the
248 misfit between the geodetic-glaciological observations is likely even larger in reality. We have
249 added a sentence to note this difference.
250
251 646-649: Suggest removal since this is an just a speculative suggestion without evidence.
252 We have clarified this point and noted that some preliminary observations, in the form of ablation
253 wires, support this point.
254

255 725: Fischer et al (2016) utilize TLS to compare detailed in-situ and geodetic observations.
256 I believe their paper supports your conclusions, though this maybe not be the
257 best placement in the paper for such a reference.
258 **This is a very interesting study and although there are parallels, we don't see a specific location**
259 **where it is logical to cite this work.**
260
261 Fausto Robert S.: A Snow Density Dataset for Improving Surface Boundary Conditions
262 in Greenland Ice Sheet Firm Modeling. *Frontiers in Earth Science*, 6,
263 DOI=10.3389/feart.2018.00051, 2018.
264
265 Fischer, M., Huss, M., Kummert, M., and Hoelzle, M.: Application and validation of
266 long-range terrestrial laser scanning to monitor the mass balance of very small glaciers
267 in the Swiss Alps, *The Cryosphere*, 10, 1279-1295, [https://doi.org/10.5194/tc-10-1279-](https://doi.org/10.5194/tc-10-1279-2016)
268 [2016](https://doi.org/10.5194/tc-10-1279-2016), 2016.
269
270 Fountain, A., and Vecchia, A.: How many stakes are required to measure the mass
271 balance of a glacier. *Geo. Ann.* 81(A), 563-568, 1999.
272
273 Mermild S and 5 others (2013) Identification of snow ablation rate, ELA, AAR and net mass
274 balance using transient snow line variations on two Arctic glaciers. *J. Glaciology*,
275 59 649-659, 2013.
276
277 Pelto, M.: Utility of late summer transient snowline migration rate on Taku Glacier,
278 Alaska, *The Cryosphere*, 5, 1127–1133, doi:10.5194/tc-5-1127-2011, 2011.
279
280 Pelto, M., Kavanaugh, J., and McNeil, C.: Juneau Icefield Mass Balance Program
281 1946–2011, *Earth Syst. Sci. Data*, 5, 319-330, [https://doi.org/10.5194/essd-5-319-](https://doi.org/10.5194/essd-5-319-2013)
282 [2013](https://doi.org/10.5194/essd-5-319-2013), 2013.
283
284 Rabatel, A.; Sirguey, P.; Drolon, V.; Maisongrande, P.; Arnaud, Y.; Berthier, E.; Davaze,
285 L.; Dedieu, J.-P.; Dumont, M. Annual and Seasonal Glacier-Wide Surface Mass Balance
286 Quantified from Changes in Glacier Surface State: A Review on Existing Methods
287 Using Optical Satellite Imagery. *Remote Sens.*, 9, 507, 2017.
288
289 Vincent, A.; Mayer, C.; Bauder, A.; Galos, A.P.; Funk, M.; Thibert, E.; Six, D.; Braun,
290 L.; Huss, M. Common climatic signal from glaciers in the European Alps over the last
291 50 years. *Geophys. Res. Lett.* 44, 2017.
292
293 WGMS 2017. Global Glacier Change Bulletin No. 2 (2014-2015). Zemp, M.,
294 Nussbaumer, S. U., Gärtner-Roer, I., Huber, J., Machguth, H., Paul, F., and Hoelzle,
295 M. (eds.), ICSU(WDS)/IUGG(IACS)/UNEP/UNESCO/WMO, World Glacier Monitoring
296 Service, Zurich, Switzerland, 244 pp., publication based on database version:
297 doi:10.5904/wgms-fog-2017-10.
298
299
300
301

302 **Interannual snow accumulation variability on glaciers derived from repeat, spatially**
303 **extensive ground-penetrating radar surveys**

304

305 Daniel McGrath¹, Louis Sass², Shad O'Neel² Chris McNeil², Salvatore G. Candela³,
306 Emily H. Baker², and Hans-Peter Marshall⁴

307 ¹*Department of Geosciences, Colorado State University, Fort Collins, CO*

308 ²*U.S. Geological Survey Alaska Science Center, Anchorage, AK*

309 ³*School of Earth Sciences and Byrd Polar Research Center, Ohio State University,*
310 *Columbus, OH*

311 ⁴*Department of Geosciences, Boise State University, Boise, ID*

312 **Abstract**

313 There is significant uncertainty regarding the spatiotemporal distribution of seasonal
314 snow on glaciers, despite being a fundamental component of glacier mass balance. To
315 address this knowledge gap, we collected repeat, spatially extensive high-frequency
316 ground-penetrating radar (GPR) observations on two glaciers in Alaska **during the spring**
317 **of** five consecutive years. GPR measurements showed steep snow water equivalent
318 (SWE) elevation gradients at both sites; continental Gulkana Glacier's SWE gradient
319 averaged 115 mm 100 m⁻¹ and maritime Wolverine Glacier's gradient averaged 440 mm
320 100 m⁻¹ (over >1000 m). We extrapolated GPR point observations across the glacier
321 surface using terrain parameters derived from digital elevation models as predictor
322 variables in two statistical models (stepwise multivariable linear regression and
323 regression trees). Elevation and proxies for wind redistribution had the greatest
324 explanatory power, and exhibited relatively time-constant coefficients over the study
325 period. Both statistical models yielded comparable estimates of glacier-wide average
326 SWE (1 % average difference at Gulkana, 4 % average difference at Wolverine),
327 although the spatial distributions produced by the models diverged in unsampled regions
328 of the glacier, particularly at Wolverine. In total, six different methods for estimating the
329 glacier-wide **winter balance** average agreed within ± 11 %. We assessed interannual
330 variability in the spatial pattern of snow accumulation predicted by the statistical models
331 using two quantitative metrics. Both glaciers exhibited a high degree of temporal
332 stability, with ~85 % of the glacier area experiencing less than 25 % normalized absolute
333 variability over this five-year interval. We found SWE at a sparse network (3 stakes per
334 glacier) of long-term glaciological stake sites to be highly correlated with the GPR-
335 derived glacier-wide average. We estimate that interannual variability in the spatial
336 pattern of **winter SWE accumulation** is only a small component (4–10 % of glacier-wide
337 average) of the total mass balance uncertainty and thus, our findings support the concept

Deleted: for

Deleted: SWE

340 that sparse stake networks effectively measure interannual variability in winter balance
341 on glaciers, rather than some [temporally](#) varying [spatial](#) pattern of snow accumulation.

342

343 **1. Introduction**

344 Our ability to quantify glacier mass balance is dependent on accurately resolving the
345 spatial and temporal distributions of snow accumulation and [snow/ice](#) ablation.

346 Significant advances in our knowledge of ablation processes have improved
347 observational and modelling capacities (Hock, 2005; Huss and Hock, 2015; Fitzpatrick et
348 al., 2017), yet comparable advances in our understanding of the distribution of snow
349 accumulation have not kept pace (Hock et al., 2017). Reasons for this discrepancy are
350 two-fold: (i) snow accumulation exhibits higher variability than ablation, both in
351 magnitude and length scale, largely due to wind redistribution in the complex high-relief
352 terrain where mountain glaciers are typically found (Kuhn et al., 1995) and (ii)
353 accumulation observations are typically less representative (i.e., one stake in a few
354 hundred meter elevation band) or less effective than comparable ablation observations
355 (i.e., precipitation gage measuring snowfall vs. radiometer measuring short-wave
356 radiation). This discrepancy presents a significant limitation to process-based
357 understanding of mass balance drivers. Furthermore, a warming climate has already
358 modified – and will continue to modify – the magnitude and spatial distribution of snow
359 on glaciers through a reduction in the fraction of precipitation falling as snow and an
360 increase in rain-on-snow events (Knowles et al., 2006; McAfee et al., 2013; Klos et al.,
361 2014; McGrath et al., 2017; Littell et al., 2018).

362

363 Significant research has been conducted on the spatial and, to a lesser degree, the
364 temporal variability of seasonal snow in mountainous and high-latitude landscapes (e.g.,
365 Balk and Elder, 2000; Molotch et al., 2005; Erickson et al., 2005; Deems et al., 2008;
366 Sturm and Wagner, 2010; Schirmer et al., 2011; Winstral and Marks, 2014; Anderson et
367 al., 2014; Painter et al., 2016). Although major advances have occurred in applying
368 physically-based snow distribution models (i.e., iSnobal (Marks et al., 1999), SnowModel
369 (Liston and Elder, 2006), Alpine 3D (Lehning et al., 2006)), the paucity of required
370 meteorological forcing data proximal to glaciers limits widespread application. Many
371 other studies have successfully developed statistical approaches that rely on the

372 relationship between the distribution of snow water equivalent (SWE) and physically-
373 based terrain parameters (also referred to as physiographic or topographic properties or
374 variables) to model the distribution of SWE across entire basins (e.g., Molotch et al.,
375 2005; Anderson et al., 2014; Sold et al., 2013; McGrath et al., 2015).

376

377 A major uncertainty identified by these studies is the degree to which these statistically
378 derived relationships remain stationary in time. Many studies (Erickson et al., 2005;
379 Deems et al., 2008; Sturm and Wagner, 2010; Schirmer et al., 2011; Winstral and Marks,
380 2014; Helfricht et al., 2014) have found ‘time-stability’ in the distribution of SWE,
381 including locations where wind redistribution is a major control on this distribution. For
382 instance, a climatological snow distribution pattern, produced from the mean of nine
383 standardized surveys, accurately predicted the observed snow depth in a subsequent
384 survey in a tundra basin in Alaska (~4–10 cm root mean square error; Sturm and Wagner,
385 2010). Repeat LiDAR surveys over two years at three hillslope-scale study plots in the
386 Swiss Alps found a high degree of correlation ($r=0.97$) in snow depth spatial patterns
387 (Schirmer et al., 2011). They found that the final snow depth distributions at the end of
388 the two winter seasons were more similar than the distributions of any two individual
389 storms during that two-year period (Schirmer et al., 2011). Lastly, an 11-year study of
390 extensive snow probing (~1200 point observations) at a 0.36 km² field site in
391 southwestern Idaho found consistent spatial patterns ($r=0.84$; Winstral and Marks, 2014).
392 Collectively, these studies suggest that in landscapes characterized by complex
393 topography and extensive wind redistribution of snow, spatial patterns are largely time-
394 stable or stationary, as long as the primary drivers are stationary.

395

396 Even fewer studies have explicitly examined the question of interannual variability in the
397 context of snow distribution on glaciers. Spatially-extensive snow probe datasets are
398 collected by numerous glacier monitoring programs (e.g., Bauder et al., 2017; Kjølmoen
399 et al., 2017; Escher-Vetter et al., 2009) in order to calculate a winter mass balance
400 estimate. Although extensive, such manual approaches are still limited by the number of
401 points that can be collected and uncertainties in correctly identifying the summer surface
402 in the accumulation zone, where seasonal snow is underlain by firn. One study of two

403 successive end-of-winter surveys of snow depth using probes on a glacier in Svalbard
404 found strong interannual variability in the spatial distribution of snow, and the
405 relationship between snow distribution and topographic features (Hodgkins et al., 2006).
406 Elevation was found to only explain 38–60 % of the variability in snow depth, and in one
407 year, snow depth was not dependent on elevation in the accumulation zone (Hodgkins et
408 al., 2006). Instead, aspect, reflecting relative exposure or shelter from prevailing winds,
409 was found to be a significant predictor of accumulation patterns. In contrast, repeat
410 airborne LiDAR surveys of a ~36 km² basin (~50% glacier cover) in Austria over five
411 winters found that the glacierized area exhibited less interannual variability (as measured
412 by the interannual standard deviation) than the non-glacierized sectors of the basin
413 (Helfricht et al., 2014). Similarly, a three-year study of snow distribution on
414 Findelgletscher in the Swiss Alps using ground-penetrating radar (GPR) found low
415 interannual variability, as 86 % of the glacier area experienced less than 25 % normalized
416 relative variability (Sold et al., 2016). These latter studies suggest that seasonal snow
417 distribution on glaciers likely exhibits ‘time-stability’ in its distribution, but few datasets
418 exist to robustly test this hypothesis.

419
420 The ‘time-stability’ of snow distribution on glaciers has particularly important
421 implications for long-term glacier mass balance programs, as seasonal and annual mass
422 balance solutions are derived from the integration of a limited number of point
423 observations (e.g., 3 to 50 stakes), and the assumption that stake and snow pit
424 observations accurately represent interannual variability in mass balance rather than
425 interannual variability in the spatial patterns of mass balance. Previous work has shown
426 ‘time-stability’ in the spatial pattern of annual mass balance (e.g., Vincent et al., 2017)
427 and while this is important for understanding the uncertainties in glacier-wide mass
428 balance estimates, the relative contributions of accumulation and ablation to this stability
429 are poorly constrained, thereby hindering a process-based understanding of these spatial
430 patterns. Furthermore, accurately quantifying the magnitude and spatial distribution of
431 winter snow accumulation on glaciers is a prerequisite for understanding the water budget
432 of glacierized basins, with direct implications for any potential use of this water, whether
433 that be ecological, agricultural, or human consumption (Kaser et al., 2010).

Deleted: R

Deleted: 15

Deleted: glacier seasonal mass balances

437

438 To better understand the ‘time-stability’ of the spatial pattern of snow accumulation on
439 glaciers, we present five consecutive years of extensive GPR observations for two
440 glaciers in Alaska. First, we use these GPR-derived SWE measurements to train two
441 different types of statistical models, which were subsequently used to spatially
442 extrapolate SWE across each glacier’s area. Second, we assess the temporal stability in
443 the resulting spatial distribution in SWE. Finally, we compare GPR-derived winter mass
444 balance estimates to traditional glaciological derived mass balance estimates and quantify
445 the uncertainty that interannual variability in spatial patterns in snow accumulation
446 introduces to these estimates.

447

448 2. Study Area

449 During the spring seasons of 2013–2017, we conducted GPR surveys on Wolverine and
450 Gulkana glaciers, located on the Kenai Peninsula and eastern Alaskan Range in Alaska
451 (Fig. 1). These glaciers have been studied as part of the U.S. Geological Survey’s
452 Benchmark Glacier project since 1966 (O’Neel et al., 2014). Both glaciers are ~16 km² in
453 area and span ~1200 m in elevation ([426 – 1635 m asl for Wolverine, 1163 – 2430 m asl](#)
454 [for Gulkana](#)). Wolverine Glacier exists in a maritime climate, characterized by warm air
455 temperatures (mean annual temperature = –0.2 °C at 990 meters; [median equilibrium line](#)
456 [altitude for 2008 – 2017 is 1235 m asl](#)) and high precipitation (median glacier-wide
457 winter balance = 2.0 m water equivalent (m w.e.)), while Gulkana is located in a
458 continental climate, characterized by colder air temperatures (mean annual temperature =
459 –2.8 °C at 1480 meters; [median equilibrium line altitude for 2008 – 2017 is 1870 m asl](#))
460 and [less](#) precipitation (median glacier-wide winter balance = 1.2 m w.e.) (Fig. 2). The
461 cumulative mass balance time series for both glaciers is negative (~ –24 m w.e. between
462 1966–2016), with Gulkana showing a more monotonic decrease over the entire study
463 interval, while Wolverine exhibited near equilibrium balance between 1966 and 1987,
464 and sharply negative to present (O’Neel et al., 2014; O’Neel et al., 2018).

465

466 3. Methods

Deleted: low

468 The primary SWE observations are derived from a GPR measurement of two-way travel
469 time (*twt*) through the annual snow accumulation layer. We describe five main steps to
470 convert *twt* along the survey profiles to annual distributed SWE products for each glacier.
471 These include (i) acquisition of GPR and ground-truth data, (ii) calculation of snow
472 density and associated radar velocity, which are used to convert measured *twt* to annual
473 layer depth and subsequently SWE, and (iii) application of terrain parameter statistical
474 models to extrapolate SWE across the glacier area. We then describe approaches to (iv)
475 evaluate the temporal consistency in spatial SWE patterns and (v) compare GPR-derived
476 SWE and direct (glaciological) winter mass balances.

477

478 **3.1. Radar data collection and processing**

479 Common-offset GPR surveys were conducted with a 500 MHz Sensors and Software
480 Pulse Ekko Pro system in late spring close to maximum end-of-winter SWE and prior to
481 the onset of extensive surface melt. GPR parameters were set to a waveform-sampling
482 rate of 0.1 ns, a 200-ns time window, and “Free Run” trace increments, where samples
483 are collected as fast as the processor allows, instead of at uniform temporal or spatial
484 increments.

485

486 In general, GPR surveys were conducted by mounting a plastic sled behind a snowmobile
487 and driving at a near-constant velocity of 15 km h⁻¹ (Fig. 3, S1, S2), resulting in a trace
488 spacing of ~20 cm. Coincident GPS data were collected using a Novatel Smart-V1 GPS
489 receiver (Omnistar corrected, L1 receiver with root-mean-square accuracy of 0.9 m
490 (Perez-Ruiz et al., 2011)). We collected a consistent survey track from year-to-year that
491 minimized safety hazards (crevasses, avalanche runouts) but optimized the sampling of
492 terrain parameter space on the glacier (e.g., range and distribution of elevation, slope,
493 aspect, curvature, etc.). However, in 2016 at Wolverine Glacier, weather conditions and
494 logistics did not allow for ground surveys to be completed. Instead, a number of radar
495 lines were collected via a helicopter survey. To best approximate the ground surveys
496 completed in other years, we selected a subset of helicopter GPR observations within 150
497 m of the ground-based surveys. Previous comparisons between ground and helicopter

498 platforms found excellent agreement in SWE point observations (coefficient of
499 determination (R^2)=0.96, root mean square error=0.14 m; McGrath et al., 2015).

500
501 Radargrams were processed using the ReflexW-2D software package (Sandmeier
502 Scientific Software). All radargrams were corrected to time zero, taken as the first
503 negative peak in the direct wave (Yelf and Yelf, 2006), and a dewow filter (mean
504 subtraction) was applied over 2 ns. When reflectors from the base of the seasonal snow
505 cover were insufficiently resolved, gain and band-pass filters were subsequently applied.
506 Layer picking was guided by ground-truth efforts and done semi-automatically using a
507 phase-following layer picker. For further details, please see McGrath et al. (2015).

Deleted: but

509 3.2. Ground truth observations

510 We collected extensive ground-truth data to validate GPR surveys, including probing and
511 snowpit/cores. In the ablation zone of each glacier, we probed the snowpack thickness
512 every ~500 m along-track. In addition, we measured seasonal snow depth and density at
513 an average of five locations (corresponding to the glaciological observations; see Section
514 3.5) on each glacier in each year. Typically these locations include one or two in the
515 ablation zone, one near the long-term ELA, and two or more in the accumulation zone.

Deleted: our

516 We measured snow density using a gravimetric approach in snowpits (at 10 cm intervals)
517 and with 7.25 cm diameter cores (if total depth >2 m; at 10–40 cm intervals depending on
518 natural breaks) to the previous summer surface. We calculated a density profile and
519 column-average density, ρ_{site} , at each site.

Deleted: at 10–40 cm intervals in each

Deleted: along

520
521 As snow densities did not exhibit a consistent spatial nor elevation dependency on the
522 glaciers (e.g., Fausto et al., 2018), we calculated a single average density, ρ , of all ρ_{site}
523 on each glacier and each year, which was subsequently used to calculate SWE:

$$525 \quad SWE = \left(\frac{twt}{2}\right) \cdot v_s \cdot \rho. \quad (1)$$

526
527 where twt is the two-way travel time as measured by the GPR and v_s is the radar
528 velocity. v_s was calculated for each glacier in each year as the average of two

533 independent approaches: (i) an empirical relationship based on the glacier-wide average ρ
534 (Kovacs et al., 1995) and (ii) a least-squares regression between snow depth derived by
535 probing and all radar *twt* observations within a 3-m radius of the probe site. An
536 exception was made at Wolverine in 2016 as no coincident probe depth observations
537 were made during the helicopter-based surveys. Instead, we estimated the second radar
538 velocity by averaging radar velocities calculated from observed *twt* and snow depths at
539 three snowpit/core locations.

540

541 3.3. Spatial Extrapolation

542 Extrapolating SWE from point measurements to the basin scale has been a topic of
543 focused research for decades (e.g., Woo and Marsh, 1978; Elder et al., 1995; Molotch et
544 al., 2005). Most commonly, the dependent variable SWE is related to a series of
545 explanatory terrain parameters, which are proxies for the physical processes that actually
546 control SWE distribution across the landscape. These include orographic gradient in
547 precipitation (elevation), wind redistribution of existing snow (slope, curvature, drift
548 potential), and aspect with respect to solar radiation and prevailing winds (eastness,
549 northness). We derived terrain parameters from 10-m resolution digital elevation models
550 (DEMs) sourced from the ArcticDEM project (Noh and Howat, 2015) for Gulkana and
551 produced from airborne Structure from Motion photogrammetry at Wolverine (Nolan et
552 al., 2015). Both DEMs were based on imagery from August 2015. Specifically, these
553 parameters include elevation, surface slope, surface curvature, northness (Molotch et al.,
554 2005), eastness, and snow drift potential (*Sb*) (Winstral et al., 2002; Winstral et al., 2013;
555 Fig. S3, S4). The *Sb* parameter is commonly used to identify locations where airflow
556 separation occurs based on both near and far-field topography and are thus likely
557 locations to accumulate snow drifts (Winstral et al., 2002). For specific details on this
558 calculation, please refer to Winstral et al. (2002). In the application of *Sb* here, we
559 determined the principle direction by calculating the modal daily wind direction during
560 the winter (October – May) when wind speeds exceeded 5 m s^{-1} (~minimum wind
561 velocity for snow transport; Li and Pomeroy, 1997). The length scales for curvature were
562 found using an optimization scheme that identified the highest model R^2 .

563

Deleted: For

Deleted: ,

Deleted: and t

Deleted: using an

568 Prior to spatial extrapolation, we aggregated GPR observations to the resolution of the
569 DEM by calculating the median value of all observations within each 10 m pixel of the
570 DEM. We then utilized two approaches to extrapolate GPR point observations across the
571 glacier surface: (i) least-squares elevation gradient applied to glacier hypsometry and (ii)
572 statistical models. For (i), we derived SWE elevation gradients in two ways; first, solely
573 on observations that followed the glacier centerline and second, from the entire spatially-
574 extensive dataset. For (ii), we utilized both stepwise multivariable linear regressions and
575 regression trees (Breiman et al., 1984). All of these approaches produced a spatially-
576 distributed SWE field over the entire glacier area. Individual points in this field are
577 equivalent to point winter balances (b_w ; m w.e.). From the distributed b_w field, we
578 calculated a mean area-averaged winter balance (B_w ; m w.e.).

579

580 Additionally, we implemented a cross-validation approach to the statistical extrapolations
581 (multivariable regression and regression tree), whereby 75 % of the aggregated
582 observations were used for training and 25 % were used for testing. However, rather than
583 randomly selecting pixels from across the entire dataset, we randomly selected a single
584 pixel containing aggregated GPR observations and then extended this selection out along
585 continuous survey lines until we reached 25 % of the total observational dataset, thus
586 removing entire sections (and respective terrain parameters) from the analysis (Fig. S5).
587 This approach provided a more realistic test for the statistical models, as the random
588 selection of individual cells did not significantly alter terrain-parameter distributions. For
589 each glacier and each year, we produced 100 training/test dataset combinations, but rather
590 than take the single model with the highest R^2 or lowest RMSE from the resulting test
591 dataset, we produced a distributed SWE product by taking the median value for each
592 pixel from all 100 model runs and a glacier-wide median value that is the median of all
593 100 individual B_w estimates. We chose the median-value approach over a highest
594 R^2 /lowest RMSE approach that is often utilized because, despite being randomly
595 selected, some training datasets were inherently advantaged by a more complete
596 distribution of terrain parameters. These iterations resulted in the highest R^2 /lowest
597 RMSE when applied to the training dataset, but weren't necessarily indicative of a better
598 model.

599

600 3.3.2. Stepwise Multivariable Linear Regression

601 We used a stepwise multivariable linear regression model of the form,

$$602 SWE_{(i,j)} = c_1x_{1(i,j)} + c_2x_{2(i,j)} + \dots + c_nx_{n(i,j)} + \varepsilon_{(i,j)}, \quad (2)$$

603 where $SWE_{(i,j)}$ is the predicted (standardized) value at location i,j and c_1, c_2, c_n are the beta
604 coefficients of the model, x_1, x_2, x_n are terrain parameters which are independent variables
605 that have been standardized and ε is the residual. We applied the regression model
606 stepwise and included an independent variable if it minimized the Akaike information
607 criterion (AIC; Akaike, 1974). We present the beta coefficients from each regression
608 (each year, each glacier) to explore the temporal stability of these terms.

609

610 3.3.3. Regression Trees

611 Regression trees (Breiman et al., 1984) provide an alternative statistical approach for
612 extrapolating point observations by recursively partitioning SWE into progressively more
613 homogenous subsets based on independent terrain parameter predictors (Molotch et al.,
614 2005; Meromy et al., 2013; Bair et al., 2018). The primary advantage of the regression
615 tree approach is that each terrain parameter is used multiple times to partition the
616 observations, thereby allowing for non-linear interactions between these terms. In
617 contrast, the MVR only allows for a single “global” linear relationship for each parameter
618 across the entire parameter-space. We implemented a random forest approach (Breiman,
619 2001) of repeated regression trees (100 learning cycles) in Matlab, using weak learners
620 and bootstrap aggregating (bagging; Breiman, 1996). Each weak learner omits 37% of
621 observations, such that these “out-of-bag” observations are used to calculate predictor
622 importance. The use of this ensemble/bagging approach reduces overfitting and thus
623 precludes having to subjectively prune the tree and provides more accurate and unbiased
624 error estimates (Breiman, 2001). Prior to implementing the regression tree, we removed
625 the SWE elevation gradient from the observations using a least-squares regression. As
626 described in the results, elevation is the dominant independent variable and as our
627 observations (particularly at Wolverine) did not cover the entire elevation range, the
628 regression tree approach was not well suited to predicting SWE at elevations outside of
629 the observational range.

630

631 3.4. Interannual variability in spatial patterns

632 We quantified the stability of spatial patterns in SWE across the five-year interval using
633 two approaches: (i) normalized range and (ii) the coefficient of determination. In the first
634 approach, we first divided each pixel in the distributed SWE fields by the glacier-wide
635 average, B_w , for each year and each glacier, and then calculated the range in these
636 normalized values over the entire five-year interval. For example, if a cell has normalized
637 values of 84 %, 92 %, 106 %, 112 % and 120 %, the normalized range would be 36 %. A
638 limitation of this approach is that it is highly sensitive to outliers, such that a single year
639 can substantially increase this range. This is similar to an approach presented by Sold et
640 al. (2016), but unlike their calculation (their Fig. 9), the normalized values reported here
641 have not been further normalized by the normalized mean of that pixel over the study
642 interval. Thus, the values reported here are an absolute normalized range, whereas Sold et
643 al. (2016) report a relative normalized range. In the coefficient of determination (R^2)
644 approach, we computed the least-squares regression correlation between the SWE in each
645 pixel and the glacier-wide average, B_w , derived from the MVR model over the five-year
646 period. For this approach, cells with a higher R^2 scale linearly with the glacier-wide
647 average, while those with low R^2 do not.

648

649 3.5. Glaciological mass balance

650 Beginning in 1966, glacier-wide seasonal (winter, B_w ; summer, B_s) and annual balances (B_a)
651 were derived from glaciological measurements made at three fixed locations on each glacier.
652 The integration of these point measurements was accomplished using a site-index method –
653 equivalent to an area-weighted average (March and Trabant, 1996; van Beusekom et al., 2010).
654 Beginning in 2009, a more extensive stake network of seven to nine stakes was established on
655 each glacier, thereby facilitating the use of a balance profile method for spatial extrapolation
656 (Cogley et al., 2011). Systematic bias in the glaciological mass balance time-series is removed
657 via a geodetic adjustment derived from DEM differencing over decadal timescales (e.g.,
658 O’Neel et al., 2014). For this study, glaciological measurements were made within a day of the
659 GPR surveys, and integrated over the glacier hypsometry using both the historically applied
660 site-index method (based on the long-term three stake network) and the more commonly

Deleted: Glacier-wide seasonal (winter, B_w ; summer, B_s) and annual balances (B_a) have been derived from sparse glaciological measurements, made at fixed locations of each glacier, since 1966. Historically, the integration of point measurements was accomplished using a site-index method – equivalent to an area-weighted average ((March and Trabant, 1996; van Beusekom et al., 2010).

Deleted: G

Deleted: each year

Deleted: a

671 applied balance profile method (based on the more extensive stake network). We utilized a
672 single glacier hypsometry, derived from the 2015 DEMs, for each glacier over the entire five-
673 year interval. **Importantly,** in order to facilitate a more direct comparison to the GPR-derived
674 B_w estimates, we used glaciological B_w estimates that have not been geodetically calibrated.

Deleted: initiated in 2009) (Cogley et al., 2011).

Deleted: I

676 4. Results

677 4.1. General accumulation conditions

678 Since 1966, Wolverine Glacier's median B_w (**determined from the stake network**) exceeds
679 Gulkana's by more than a factor of two (2.3 vs. 1.1 m w.e.), and exhibits greater
680 variability, with an interquartile range more than twice as large (0.95 m w.e. vs. 0.4 m
681 w.e.). Over the five-year study period, both glaciers experienced accumulation conditions
682 that spanned their historical ranges, with one year in the upper quartile (including the 5th
683 greatest B_w at Wolverine in 2016), one year within 25% of the median, and multiple years
684 in the lower quartile (2017 at Gulkana and 2014 at Wolverine had particularly low B_w
685 values) (Fig. 2). In all years, B_w at Wolverine was greater, although in 2013 and 2014, the
686 difference was only 0.1 m w.e.

687
688 Average accumulation season (taken as October 1 – May 31) wind speeds over the study
689 period were stronger (~ 7 m s^{-1} vs. ~ 3 m s^{-1}) and from a more consistent direction at
690 Wolverine than Gulkana (northeast at Wolverine, southwest to northeast at Gulkana)
691 (Fig. S6). On average, Wolverine experienced ~ 50 days with wind gusts >15 m s^{-1} each
692 winter, while for Gulkana, this only occurred on ~ 7 days. Over the five-year study period,
693 interannual variability in wind direction was very low at Wolverine (2016 saw slightly
694 greater variability, with an increase in easterly winds). In contrast, at Gulkana, winds
695 were primarily from the northeast to east in 2013–2015, from the southwest to south in
696 2016–2017, and experienced much greater variability during any single winter.

698 4.2. *In situ* and GPR point observations

699 Glacier-averaged snow densities across all years were 440 kg m^{-3} (range 414–456 kg m^{-3})
700 at Wolverine and 362 kg m^{-3} (range 328–380 kg m^{-3}) at Gulkana (Table S1). Average
701 radar velocities were 0.218 m ns^{-1} (range 0.207–0.229 m ns^{-1}) at Wolverine and 0.223 m

704 ns^{-1} (0.211–0.231 m ns^{-1}) at Gulkana. Over this five-year interval, the GPR point
705 observations revealed a general pattern of increasing SWE with elevation, along with
706 fine-scale variability due to wind redistribution (e.g., upper elevations of Wolverine) and
707 localized avalanche input (e.g., lower west branch of Gulkana) (Fig. S1, S2). The
708 accumulation season (hereafter, winter) SWE elevation gradient was steeper (~ 440 vs.
709 ~ 115 $\text{mm } 100 \text{ m}^{-1}$) and more variable in its magnitude at Wolverine than Gulkana.
710 Gradients ranged between 348 – 624 $\text{mm } 100 \text{ m}^{-1}$ at Wolverine, and 74 – 154 $\text{mm } 100 \text{ m}^{-1}$
711 at Gulkana (Fig. 4). Over all five years at both glaciers, elevation explained between 50
712 % and 83 % of the observed variability in SWE (Fig. 4).

713

714 **4.3. Model performance**

715 To evaluate model performance in unsampled locations of the glacier, both extrapolation
716 approaches were run 100 times for each glacier and each year, each time with a unique,
717 randomly selected training (75 % of aggregated observations) and test (remaining 25 %
718 of aggregated observations) dataset. The median and standard deviation of the
719 coefficients of determination (R^2) from these 100 models runs are shown in Fig. 5. Model
720 performance ranged from 0.25 to 0.75, but on average, across both glaciers and all years,
721 was 0.56 for the MVR approach and 0.46 for the regression tree. Model performance was
722 higher and more consistent at Wolverine, whereas 2015 and 2017 at Gulkana had test
723 dataset R^2 of ~ 0.4 and 0.3, likely reflecting the lower winter SWE elevation gradients and
724 coefficients of determination with elevation during these years (Fig. 4). The wide range
725 in R^2 across the 100 model runs reflects the variability in training and test datasets that
726 were randomly selected. When the test dataset terrain parameter space was captured by
727 the training dataset, a high coefficient of determination resulted, but when the test dataset
728 terrain parameter space was exclusive, e.g., contained only a small elevation range, the
729 model performance was typically low. This further highlights the importance of elevation
730 as a predictor for these glaciers.

731

732 At Gulkana, the model residuals (Fig. S1) exhibited spatiotemporal consistency, with
733 positive residuals (i.e., observed SWE exceeded modeled SWE by $\sim 0.2 \text{ m w.e.}$) at mid-
734 elevations of the west branch, and at the very terminus of the glacier. The largest negative

735 residuals typically occurred at the highest elevations. In both cases, these locations
736 deviated from the overall SWE elevation gradient. At Wolverine, observations at the
737 highest elevations typically exceeded the modeled SWE, particularly in the northeast
738 quadrant of the glacier where wind drifting is particularly prevalent (Fig. S2). Elsewhere
739 at Wolverine, the residuals often alternated between positive and negative values over
740 length scales of 10s to 100s of meters (Fig. S2), which we interpret as zones of scour/drift
741 that were better captured by the regression tree models.

742

743 The beta coefficients of terrain parameters from the MVR were fairly consistent from
744 year-to-year at both glaciers (Fig. 6). At Wolverine, elevation was the largest beta
745 coefficient, followed by *Sb* and curvature. At Gulkana, elevation was also the largest beta
746 coefficient, followed by curvature. Gulkana experiences much greater variability in wind
747 direction during the winter months (Fig. S6), possibly explaining why *Sb* was either not
748 included or had a very low beta coefficient in the median regression model. As our
749 surveys were completed prior to the onset of ablation, terrain parameters related to solar
750 radiation gain (notably the terms that include aspect: northness and eastness) had small
751 and variable beta coefficients.

752

753 **4.4. Spatial Variability**

754 A common approach for quantifying snow accumulation variability across a range of
755 means is the coefficient of variation (CoV), calculated as the ratio of the standard
756 deviation to the mean (Liston et al., 2004; Winstral and Marks, 2014). The mean and
757 standard deviation of CoVs at Wolverine were 0.42 ± 0.03 and at Gulkana, 0.29 ± 0.05 ,
758 indicating relatively lower spatial variability in SWE at Gulkana (Fig. 7). CoVs were
759 fairly consistent across all five years, although 2017 saw the largest CoVs at both
760 glaciers. Interestingly, 2017 had the lowest absolute spatial variability (i.e., lowest
761 standard deviation), but also the lowest glacier-wide averages during the study period,
762 resulting in greater CoVs.

763

764 Qualitatively, both Wolverine and Gulkana glaciers exhibited consistent spatiotemporal
765 patterns in accumulation across the glacier surface, with elevation exerting a first-order

766 control (Fig. 8, S7, S8). Overlaid on the strong elevational gradient are consistent
767 locations of wind scour and deposition, reflecting the interaction of wind redistribution
768 and complex – albeit relatively stable year to year – surface topography (consisting of
769 both land and ice topography). For instance, numerous large drifts (~2 m amplitude, ~200
770 m wavelength) occupy the northeast corner of Wolverine Glacier, where prevailing
771 northeasterly winds consistently redistributed snow into sheltered locations in each year
772 of the study period (Fig. 8). The different statistical extrapolation approaches produced
773 nearly identical B_w estimates (4 % difference on average at Wolverine and 1 % difference
774 on average at Gulkana) (Fig. 9). The MVR B_w estimate was larger in 4 out of 5 years at
775 Wolverine (Fig. 9), while neither approach exhibited a consistent bias at Gulkana.

776

777 Although the glacier-wide averages between these approaches showed close agreement,
778 we explored the differences in spatial patterns by calculating a mean SWE difference
779 map for each glacier by differencing the five-year mean SWE produced by the
780 regression tree model ~~from the same produced by the MVR model~~ (Fig. 10). As such,
781 locations where the MVR exceeded the regression tree are positive (yellow). At Gulkana,
782 where the two approaches showed slightly better glacier-wide B_w agreement, the
783 magnitude in individual pixel differences were substantially less than at Wolverine (e.g.,
784 color bar scales range ± 0.2 m at Gulkana vs. ± 0.5 m at Wolverine). At Wolverine
785 Glacier, there were three distinct elevation bands where the MVR approach predicted
786 greater SWE, namely the main icefall in the ablation zone, a region of complex
787 topography centered around a normalized elevation of 0.65, and lastly, at higher
788 elevations, where both approaches predicted a series of drift and scour zones, although in
789 sum, the MVR model predicted greater SWE.

790

791 We used two different approaches to quantify the ‘time-stability’ of spatial patterns
792 across these glaciers. By the first metric, normalized range, we found that both glaciers
793 exhibited very similar patterns (Fig. 11), with either ~65 or 85 % (regression tree and
794 MVR, respectively) of the glacier area experiencing less than 25 % absolute normalized
795 variability (Fig. 12). The R^2 approach provides an alternative way of assessing the time
796 stability of SWE, essentially determining whether SWE at each location scales with the

Deleted: form

798 glacier-wide value. By this metric, 80 % of the glacier area at Wolverine and 96 % of the
799 glacier area at Gulkana had a coefficient of determination greater than 0.8 (Fig. 12),
800 suggesting that most locations on the glacier have a consistent relationship with the mean
801 glacier-wide mass balance. By both metrics, the MVR output suggests greater ~~‘time-~~
802 stability’ (e.g., lower normalized range or higher R^2) compared to the regression tree.
803

Deleted: temporal

804 4.5. Winter mass balance

805 In order to examine systematic variations between the approaches we outlined in Section
806 3 for calculating the glacier-wide winter balance, B_w , we first calculated a yearly mean
807 from the six approaches (including four based on the GPR observations: MVR,
808 regression tree, elevation gradient derived from centerline only observations, elevation
809 gradient derived from all point observations, and two based on the *in situ* stake network:
810 site-index and profile). In general, Gulkana exhibited greater agreement (4 % average
811 difference) among the approaches, with most approaches agreeing within 5 % of the six-
812 approach mean (Fig. 13; Table S2). Wolverine showed slightly less agreement (7 %
813 average difference), as the two terrain parameters statistical extrapolations (MVR and
814 regression tree) produced B_w estimates ~9 % above the mean, while the two stake derived
815 estimates were ~7 % less than the mean. On average across all five years at Wolverine,
816 the MVR approach was the most positive, while the glaciological site-index approach
817 was always the most negative (Fig. 13). At both glaciers, the estimates using elevation as
818 the only predictor yielded B_w estimates on average within 3 % of the six-method mean,
819 with the centerline only based estimate being slightly negatively biased, and the complete
820 observations being slightly positively biased.

821
822 To examine the systematic difference between the glaciological site-index method and
823 GPR-based MVR approach, we compared stake-derived b_w values from the three long-
824 term stakes to all GPR-based MVR b_w values within that index zone (Fig. 14). Both the
825 stakes and the GPR-derived b_w values have been normalized by the glacier-wide value to
826 make these results comparable across years and glaciers. It is apparent that Wolverine
827 experienced much greater spatial variability in accumulation, with larger interquartile
828 ranges and a large number of positive outliers in all index zones. Importantly, the stake

830 weight in the site-index solution is dependent on the hypsometry of the glacier, and for
831 both glaciers, the upper stake accounts for ~65 % of the weighted average. In years that
832 the misfit between GPR B_w and site-index B_w was largest (2015 and 2016 at Gulkana,
833 2013 and 2017 at Wolverine), the stake-derived b_w at the upper stake was in the lower
834 quartile of all GPR-derived b_w values, explaining the significant difference in B_w
835 estimates in these years. Potential reasons for this discrepancy are discussed in Section
836 5.3.

837

838 *In situ* stake and pit observations traditionally serve as the primary tool for deriving
839 glaciological mass balances. However, in order for these observations to provide a
840 systematic and meaningful long-term record, they need to record interannual variability
841 in mass balance rather than interannual spatial variability in mass balance. To assess the
842 performance of the long-term stake sites, we examined the interannual variability metrics
843 for the stake locations. By both metrics (normalized absolute range and R^2), the middle
844 and upper elevation stakes at both glaciers appear to be in locations that achieve this
845 temporal stability, having exhibited ~10 % range and $R^2 > 0.95$ over the five-year interval.
846 The lower elevation stake was less temporally stable and exhibited opposing behavior at
847 each glacier. At Gulkana, this stake had a high R^2 (0.93) and moderate normalized
848 variability (26 %), which in part, reflects the lower total accumulation at this site and the
849 ability for a single uncharacteristic storm to alter this total amount significantly. In
850 contrast, Wolverine's lowest site exhibited both low R^2 (<0.01) and normalized range (2
851 %), a somewhat unlikely combination. The statistical extrapolation approaches frequently
852 predicted zero or near-zero cumulative winter accumulation at this site (i.e., mid-winter
853 rain and/or ablation is common at this site), so although the normalized range was quite
854 low, predicted SWE values were uncorrelated with B_w over the study interval.

855

856 **Discussion**

857 **5.1. Interannual variability in spatial patterns**

858 Each glacier exhibited consistent normalized SWE spatial patterns across the five-year
859 study, reflecting the strong control of elevation and regular patterns in wind redistribution
860 in this complex topography (Fig. 11, S7, S8). This is particularly notable given the highly

861 variable magnitudes of accumulation over the five-year study and the contrasting climate
862 regions of these two glaciers (wet, warm maritime and cold, dry continental), with unique
863 storm paths, timing of annual accumulation, wind direction and wind direction
864 variability, and snow density. At both glaciers, the lowest interannual variability was
865 found away from locations with complex topography and elevated surface roughness,
866 such as crevassed zones, glacier margins, and areas near peaks and ridges.

867

868 In the most directly comparable study using repeat GPR surveys at Switzerland's
869 Findelgletscher, 86 % of the glacier area experienced less than 25 % range in relative
870 normalized accumulation over a three-year interval (Sold et al., 2016). As noted in
871 Section 3.4., we reported an absolute normalized range, whereas Sold et al. (2016)
872 reported a relative normalized range. Following their calculation, we found that 81 and
873 82 % of Wolverine and Gulkana's area experienced a relative normalized range less than
874 25 %. Collectively, our results add to the growing body of evidence (e.g., Deems et al.,
875 2008; Sturm and Wagner, 2010; Schirmer et al., 2011; Winstral and Marks, 2014)
876 suggesting 'time-stability' in the spatial distribution of snow in locations that span a
877 range of climate zones, topographic complexity, and relief. While the initial effort
878 required to constrain the spatial distribution over a given area can be significant, the
879 benefits of understanding the spatial distribution are substantial and long-lasting, and
880 have a wide range of applications.

881

882 5.1.1 Elevation

883 Elevation explained between 50 and 83 % of the observed SWE variability at Gulkana
884 and Wolverine, making it the most significant terrain parameter at both glaciers every
885 year (Fig. 4, 6). ~~Steep winter SWE gradients characterized both glaciers throughout the~~
886 ~~study period (115 – 440 mm 100 m⁻¹). Such gradients are comparable to previous results~~
887 ~~for glaciers in the region (Pelto, 2008; Pelto et al., 2013; McGrath et al., 2015), but~~
888 ~~exceed reported orographic precipitation gradients in other mountainous regions by a~~
889 factor of 2–3 (e.g., Anderson et al., 2014; Grünewald and Lehning, 2011). These steep
890 gradients are ~~likely the~~ result of physical processes beyond just orographic precipitation,
891 including storm systems that deliver snow at upper elevations and rain at lower elevations

Deleted: Exceptionally s

Deleted: SWE

Deleted: ,

Formatted: Superscript

Deleted: annually exceeding reported

Deleted: the

897 (common at both Wolverine and Gulkana) and mid-winter ablation at lower elevations (at
898 Wolverine). These processes have also been shown to steepen observed SWE gradients
899 relative to orographic precipitation gradients in a mid-latitude seasonal snow watershed
900 (Anderson et al., 2014). Unfortunately, given that we solely sampled snow distribution at
901 the end of the accumulation season, the relative magnitude of each of these secondary
902 processes is not constrained.

Deleted: poorly

904 Wolverine and Gulkana glaciers exhibited opposing SWE gradients at their highest
905 elevations, with Wolverine showing a sharp non-linear increase in SWE, while Gulkana
906 showed a gradual decrease. This non-linear increase was also noted at two maritime
907 glaciers (Scott and Valdez) in 2013 (McGrath et al., 2015), and perhaps reflects an
908 abundance of split precipitation phase storms in these warm coastal regions. The cause of
909 the observed reverse gradient at Gulkana may be the result of wind scouring at the
910 highest and most exposed sections of the glacier, or in part, a result of where we were
911 able to safely sample the glacier. For instance, in 2013, when we were able to access the
912 highest basin on the glacier, the SWE elevation gradient remained positive (Fig. 4).
913 Reductions in accumulated SWE at the highest elevations have also been observed at
914 Lemon Creek Glacier in southeast Alaska and Findel Glacier in Switzerland (Machguth
915 et al., 2006), presumably related to wind scouring at these exposed elevations.

Deleted: behavior

Deleted: other

917 5.1.2. Wind redistribution

918 Both statistical extrapolation approaches found terrain parameters Sb and curvature,
919 proxies for wind redistribution, to have the largest beta coefficients after elevation (Fig.
920 6, S9). The spatial pattern of SWE estimated by each model clearly reflects the dominant
921 influence of wind redistribution and elevation (Fig. 8), as areas of drift and scour are
922 apparent, especially at higher elevations. However, these terms do not fully capture the
923 redistribution process, as the model residuals (Fig. S1, S2) show sequential positive and
924 negative residuals associated with drift/scour zones. There are a number of reasons why
925 this might occur, including variable wind directions transporting snow (this is likely a
926 more significant issue at Gulkana, which experiences greater wind direction variability
927 (Fig. S6)), complex wind fields that are not well represented by a singular wind direction

931 (Dadic et al., 2010), changing surface topography (the glacier surface is dynamic over a
932 range of temporal scales, changing through both surface mass balance processes and ice
933 dynamics), and widely varying wind velocities. This is particularly relevant at Wolverine,
934 where wind speeds regularly gust over 30 m s^{-1} during winter storms, speeds that result in
935 variable length scales of redistribution that would not be captured by a fixed length scale
936 of redistribution. All of these factors influence the redistribution of snow and limit the
937 predictive ability of relatively simple proxies. Significant effort has gone into developing
938 physically-based snow-distribution models (e.g., Alpine3D and SnowModel), however,
939 high-resolution meteorological forcing data requirements generally limit the application
940 of these models in glacierized basins. Where such observations do exist, previous studies
941 have illuminated how the final distribution of snow is strongly correlated to the complex
942 wind field, including vertical (surface normal) winds (Dadic et al., 2010).

943

944 5.1.3. Differences with non-glaciated terrain

945 Although our GPR surveys did not regularly include non-glaciated regions of these
946 basins, a few key differences are worth noting. First, the length scales of variability on
947 and off the glacier were distinctly different, with shorter scales and greater absolute
948 variability (snow-free to $>5 \text{ m}$ in less than 10 m distance) off-glacier (Fig. S10). This
949 point has been clearly shown using airborne LiDAR in a glaciated catchment in the
950 Austrian Alps (Helfricht et al., 2014). The reduced variability on the glacier is largely due
951 to surface mass balance and ice flow processes that act to smooth the surface, leading to a
952 more spatially consistent surface topography, and therefore a more spatially consistent
953 SWE pattern. For this reason, establishing a SWE elevation gradient on a glacier is likely
954 much less prone to terrain-induced outliers compared to off-glacier sites, although the
955 relationship of this gradient to off-glacier gradients is generally unknown.

956

957 5.2. Spatial differences between statistical models

958 The two statistical extrapolation approaches yielded comparable large-scale spatial
959 distributions and glacier-wide averages, although there were some notable spatial
960 differences (Fig. 10). The systematic positive bias of the MVR approach over the
961 regression tree at Wolverine was due to three sectors of the glacier with both complex

Deleted: In that way, measuring mean snowfall at a specific elevation and establishing the elevation gradient in SWE on a glacier is often much less prone to terrain-induced outliers (if obvious outlier locations, like icefalls, are avoided) than it is off-glacier.

967 terrain (i.e., icefalls) and large data gaps (typically **locations that are** not safe to access on
968 ground surveys). The difference in predicted SWE in these locations is likely due to how
969 the two statistical extrapolation approaches handle unsampled terrain parameter space.
970 The MVR extrapolates based on global linear trends, while the regression tree assigns
971 SWE from terrain that most closely resembles the under-sampled location. Anecdotally,
972 it appears that the MVR may overestimate SWE in some of these locations, which is most
973 evident in Wolverine's lower icefall, where bare ice is frequently exposed at the end of
974 the accumulation season (Fig. S11) in locations where the MVR predicted substantial
975 SWE. Likewise, the regression tree models could be underestimating SWE in these
976 regions, but in the absence of direct observations the errors are inherently unknown. The
977 regression tree model captures more short length scale variability while the MVR model
978 clarifies the larger trends. Consequently, smaller drifts and scours are captured well by
979 the regression tree model in areas where the terrain parameter space is well surveyed, but
980 the results become progressively less plausible as the terrain becomes more different
981 from the sampled terrain parameter space. In contrast, the MVR model appears to give
982 more plausible results at larger spatial scales. This suggests that there is some theoretical
983 threshold where the regression tree is more appropriate if the terrain parameter space is
984 sampled sufficiently, but that for many glacier surveys the MVR model would be more
985 appropriate.

986

987 **5.3. Winter mass balance comparisons**

988 On average, all methods for estimating B_w were within $\pm 11\%$ of the six-method mean,
989 (Fig. 13). The agreement (as measured by the average percent difference from the mean)
990 between estimates was slightly better at Gulkana than Wolverine, likely reflecting the
991 overall lower spatial variability at Gulkana and the greater percentage of the glacier area
992 where b_w correlates well with the glacier-wide average (Fig. 11 e, f). At both glaciers, B_w
993 solutions based solely on elevation showed excellent agreement to the six-method mean,
994 suggesting that this simple approach is a viable means for measuring B_w on these glaciers.
995 The biggest differences occurred between the GPR-forced MVR model and the
996 glaciological site-index method, which we've shown is attributed to the upper stake (with
997 the greatest weight) underestimating the median SWE for that index zone (Fig. 14). The

998 upper stake location was established in 1966 at an elevation below the median elevation
999 of that index zone, which given the strong elevation control on SWE, is a likely reason
1000 for the observed difference. At Gulkana, the relationship between the upper index site
1001 and the GPR-forced MVR model is more variable in large part due to observed
1002 differences in the accumulation between the main branch (containing the index site) and
1003 the west branch of the glacier (containing additional stakes added in 2009). Such basin-
1004 scale differences are likely present on many glaciers with complex geometry, and thus
1005 illustrate potential uncertainties of using a small network of stakes to monitor the mass
1006 balance of these glaciers. In the context of the MVR model, this manifests as a change in
1007 sign in the eastness coefficient (which separates the branches in parameter space; Fig.
1008 S4). Notably, in the two years where the site-index estimate was most negatively biased
1009 at Gulkana (2015 and 2016), the glaciological profile method, relying on the more
1010 extensive stake network (which includes stakes in the west branch of the glacier), yielded
1011 B_w estimates within a few percent of the GPR-derived MVR estimate.

1012
1013 These GPR-derived B_w results have important implications for the cumulative
1014 glaciological (stake-derived) mass balance time-series (currently only based on the site-
1015 index method), which is calibrated with geodetic observations (O'Neel et al., 2014). It is
1016 important to remember that the previous comparisons (e.g., Fig. 13) were based on
1017 glaciological B_w values that have not had a geodetic calibration applied. At Wolverine,
1018 the cumulative annual glaciological mass balance solutions are positively biased
1019 compared to the geodetic mass balance solutions over decadal timescales, requiring a
1020 negative calibration (-0.43 m w.e. a^{-1} ; O'Neel et al., 2014) to be applied to the
1021 glaciological solutions. The source of this disagreement is some combination of the
1022 stake-derived winter and summer balances being too positive relative to the geodetic
1023 solution. On average, the GPR-derived B_w results were ~ 0.4 m w.e. more positive than the
1024 site-index B_w results at Wolverine, which would further increase the glaciological-
1025 geodetic solution difference and suggest that the stake-derived glaciological solutions are
1026 underestimating ablation (B_s) by ~ 0.8 m w.e. a^{-1} . Preliminary observations at Wolverine
1027 using ablation wires show that some sectors of the glacier experience very high ablation
1028 rates that are not captured by the stake network (e.g., crevassed zones through enhanced

Deleted: If the GPR-derived solutions are assumed to be the most accurate estimate of B_w , this misfit would be further increased by -0.4 m w.e. a^{-1} (the mean difference between MVR and site-index B_w estimates), suggesting that the stakes are underestimating ablation (B_s) by ~ 1 m w.e. a^{-1} . This suggests

1035 shortwave solar radiation gain (e.g., Pfeffer and Bretherton, 1987; Cathles et al., 2011;
1036 Colgan et al., 2016), and/or increased turbulent heat fluxes due to enhanced surface
1037 roughness), and/or ice margins (through enhanced longwave radiation from nearby snow-
1038 free land cover)). However, these results are not universal, as the assimilation of
1039 distributed GPR observations at Findelgletcher significantly improved the comparison
1040 between geodetic and modeled mass balance estimates (Sold et al., 2016), suggesting
1041 multiple drivers of glaciologic-geodetic mismatch for long-term mass balance programs.

1042

1043 **5.3.1. Implications for stake placement**

1044 Understanding the spatiotemporal distribution of SWE is useful for informing stake
1045 placements and also for quantifying the uncertainty that interannual spatial variations in
1046 SWE introduce to historic estimates of glacier-wide mass balance, particularly when
1047 long-term mass balance programs rely on limited numbers of point observations (e.g.,
1048 USGS and National Park Service glacier monitoring programs; O’Neel et al., 2014;
1049 Burrows, 2014). Our winter balance results illustrate that stakes placed at the same
1050 elevation are not directly comparable, and hence are not necessarily interchangeable in
1051 the context of a multi-year mass balance record. Most locations on the glacier exhibit bias
1052 from the average mass balance at that elevation and our results suggest interannual
1053 consistency in this bias over sub-decadal time scales. As a result, constructing a balance
1054 profile using a small number of inconsistently located stakes is likely to introduce large
1055 relative errors from one year to the next.

1056

1057 Considering this finding, the placement of stakes to measure snow accumulation is
1058 dependent on whether a single glacier-wide winter mass balance value (B_w) or a spatially
1059 distributed SWE field is desired as a final product. For the former, a small number of
1060 stakes can be distributed over the glacier hypsometry in areas where interannual
1061 variability is low. Alternatively, if a distributed field is desired, a large number of stakes
1062 can be widely distributed across the glacier, including areas where the interannual
1063 variability is higher. In both cases it is important to have consistent locations from year to
1064 year, although as the number of stakes increases significantly, this becomes less critical.

1065

1066 We assess the uncertainty that interannual variability in the spatial distribution of SWE
1067 introduces to the historic index-method (March and Trabant, 1996) mass balance
1068 solutions by first calculating the uncertainty, σ , contributed by each stake as:

$$1069 \sigma_{stake} = \sigma_{model\ residuals} + (1 - r^2) \cdot u, \quad (3)$$

1070 where $\sigma_{model\ residuals}$ is the standard deviation of MVR model residuals over all five
1071 years within ± 30 meters of the index site, u is the mean b_w within ± 30 meters of the
1072 index site, and R^2 is the coefficient of determination between b_w and B_w over the five-year
1073 period (Fig. 11). The first term on the right hand side of Eq. 3 accounts for both the
1074 spatial and temporal variability in the observed b_w as compared to the model, and the
1075 second term accounts for the variability of the model as compared to B_w . The glacier-
1076 wide uncertainty from interannual variability is then:

$$1077 \text{Glacier } \sigma = \sqrt{\sum_{all\ stakes} (\sigma_{stake} \cdot w_{stake})^2}, \quad (4)$$

1078 where w_{stake} is the weight function from the site-index method (which depends on stake
1079 location and glacier hypsometry). By this assessment, interannual variability in the spatial
1080 distribution of SWE at stake locations introduced minor uncertainty, on the order of 0.11
1081 m w.e. at both glaciers (4 % and 10 % of B_w at Wolverine and Gulkana, respectively).
1082 This suggests that the original stake network design at the benchmark glaciers does
1083 remarkably well at capturing the interannual variability in glacier-wide winter balance.
1084 The greatest interannual variability at each glacier is found at the lowest stake sites, but
1085 because b_w and the stake weights are both quite low at these sites, they contribute only
1086 slightly to the overall uncertainty. Instead, the middle and upper elevation stakes
1087 contribute the greatest amount to the glacier-wide uncertainty.

1088

1089 **6. Conclusions**

1090 We collected spatially extensive GPR observations at two glaciers in Alaska for five
1091 consecutive winters to quantify the spatiotemporal distribution of SWE. We found good
1092 agreement of glacier-average winter balances, B_w , among the four different approaches
1093 used to extrapolate GPR point measurements of SWE across the glacier hypsometry.
1094 Extrapolations relying only on elevation (i.e., a simple balance profile) produced B_w
1095 estimates similar to the more complicated statistical models, suggesting that this is an
1096 appropriate method for quantifying glacier-wide winter balances at these glaciers. The

1097 more complicated approaches, which allow SWE to vary across a range of terrain-
1098 parameters based on DEMs, show a high degree of temporal stability in the pattern of
1099 accumulation at both glaciers, as ~85 % of the area on both glaciers experienced less than
1100 25 % normalized absolute variability over the five-year interval. Elevation and the
1101 parameters related to wind redistribution had the most explanatory power, and were
1102 temporally consistent at each site. The choice between MVR and regression tree models
1103 should depend on both the range in terrain-parameter space that exists on the glacier,
1104 along with how well that space is surveyed.

1105

1106 In total, six different methods (four based on GPR measurements and two based on stake
1107 measurements) for estimating the glacier-wide average agreed within ± 11 %. The site-
1108 index glaciological B_w estimates were negatively biased compared to all other estimates,
1109 particularly when the upper-elevation stake significantly underestimated SWE in that
1110 index zone. In contrast, the profile glaciological approach, using a more extensive stake
1111 network, showed better agreement with the other approaches, highlighting the benefits of
1112 using a more extensive stake network.

1113

1114 We found the spatial patterns of snow accumulation to be temporally stable on these
1115 glaciers, which is consistent with a growing body of literature documenting similar
1116 consistency in a wide variety of environments. The long-term stake locations experienced
1117 low interannual variability in normalized SWE, meaning that stake measurements tracked
1118 the interannual variability in SWE, rather than interannual variability in spatial patterns.
1119 The uncertainty associated with interannual spatial variability is only 4–10 % of the
1120 glacier-wide B_w at each glacier. Thus, our findings support the concept that sparse stake
1121 networks can be effectively used to measure interannual variability in winter balance on
1122 glaciers.

1123

1124 *Data Availability.* The GPR and associated observational data used in this study can be
1125 accessed on the USGS Glaciers and Climate Project website
1126 (<https://doi.org/10.5066/F7M043G7>). The Benchmark Glacier mass balance input and
1127 output can be accessed at: <https://doi.org/10.5066/F7HD7SRF> (O’Neel et al., 2018). The

Deleted: will be

1128 Gulkana DEM is available from the ArcticDEM project website
1129 (<https://www.pgc.umn.edu/data/arcticdem/>) and the Wolverine DEM ~~js~~ available at
1130 <ftp://bering.gps.alaska.edu/pub/chris/wolverine/>. A generalized version of the SWE
1131 extrapolation code is available at: [Distribution](https://github.com/danielmcgrathCSU/Snow-</u>
1132 <u><a href=).

1133
1134 *Author Contributions.* SO, DM, LS, and HPM designed the study. DM performed the
1135 analyses and wrote the manuscript. LS contributed to the design and implementation of
1136 the analyses, and CM, SC, and EHB contributed specific components of the analyses. All
1137 authors provided feedback and edited the manuscript.

1138
1139 *Competing Interests.* The authors declare that they have no conflict of interest.

1140
1141 *Acknowledgments.* This work was funded by the U.S. Geological Survey Land Change
1142 Science Program, USGS Alaska Climate Adaptation Science Center, and DOI/USGS
1143 award G17AC00438 to DM. Any use of trade, firm, or product names is for descriptive
1144 purposes only and does not imply endorsement by the U.S. Government. We
1145 acknowledge the Polar Geospatial Center (NSF-OPP awards 1043681, 1559691, and
1146 1542736) for the Gulkana DEM. We thank Caitlyn Florentine, Jeremy Littell, Mauri
1147 [Pelto, and an anonymous reviewer for their thoughtful feedback that improved the](#)
1148 [manuscript](#).

1149 **References**

1151
1152 Akaike, H.: A new look at the statistical model identification, IEEE Trans. Autom.
1153 Control, AC-19(6), 1974.
1154
1155 Anderson, B. T., McNamara, J. P., Marshal, H. P., and Flores, A. N.: Insights into the
1156 physical processes controlling correlations between snow distribution and terrain
1157 properties, Water Res. Res., 50(6), 4545–4563, doi:10.1002/2013WR013714, 2014.
1158
1159 [Bauder, A. \(ed\): The Swis Glaciers, 2013/14 and 2014/15, Glaciological Report \(Glacier\)](#)
1160 [No. 135/136, doi:10.18752/glrep_135-136, 2017.](#)

1162
1163 Bair, E. H., Calfa, A.A., Rittger, K., and Dozier, J.: Using machine learning for real-time
1164 estimates of snow water equivalent in the watersheds of Afghanistan, *The Cryosphere*,
1165 12, 1579–1594, doi:10.5194/tc-12-1579-2018, 2018.
1166
1167 Balk, B. and Elder, K.: Combining binary regression tree and geostatistical methods to
1168 estimate snow distribution in a mountain watershed, *Water Res. Res.*, 36(1), 13–26, 2000.
1169
1170 Burrows, R.: Annual report on vital signs monitoring of glaciers in the Central Alaska
1171 Network 2011–2013, Natural Resource Technical Report NPS/CAKN/NRTR—2014/905,
1172 National Park Service, Fort Collins, Colorado, 2014.
1173
1174 Breiman, L.: Bagging predictors, *Mach. Learn.*, 24, 123–140,
1175 <https://doi.org/10.1023/A:1018054314350>, 1996.
1176
1177 Breiman, L.: Random forests, *Mach. Learn.*, 45, 5–32,
1178 <https://doi.org/10.1023/A:1010933404324>, 2001.
1179
1180 Breiman, L., Friedman, J. H., Olshen, R. A., and Stone, C. J.: *Classification and*
1181 *Regression Trees*, Chapman and Hall, New York, 368 pp., 1984.
1182
1183 Cathles, L. C., Abbot, S. D., Bassis, J. N., and MacAyeal, D.R.: Modeling surface-
1184 roughness/solar-ablation feedback: application to small-scale surface channels and
1185 crevasses of the Greenland ice sheet, *Ann. Glaciol.*, 52(59), 99–108, 2011.
1186
1187 Cogley, J. G., Hock, R., Rasmussen, L. A., Arendt, A. A., Bauder, A., Braithwaite, R. J.,
1188 Jansson, P., Kaser, G., Möller, M., Nicholson, L. and Zemp, M.: *Glossary of Glacier*
1189 *Mass Balance and Related Terms*, IHP-VII Technical Documents in Hydrology No. 86,
1190 IACS Contribution No. 2, UNESCO-IHP, Paris, 2011.
1191

1192 Colgan, W., Rajaram, H., Abdalati, W., McCutchan, C., Mottram, R., Moussavi, M. S.,
1193 and Grigsby, S.: Glacier crevasses: Observations, models, and mass balance implications,
1194 *Rev. Geophys.*, 54, doi:10.1002/2015RG000504, 2016.

1195

1196 Dadic, R., Mott, R., Lehning, M., and Burlando, P.: Wind influence on snow depth
1197 distribution and accumulation over glaciers, *J. Geophys. Res.*, 115, F01012,
1198 doi:10.1029/2009JF001261, 2010.

1199

1200 Deems, J. S., Fassnacht, S. R., and Elder, K. J.: Interannual consistency in fractal snow
1201 depth patterns at two Colorado mountain sites, *J. Hydromet.*, 9, 977–988,
1202 doi:10.1175/2008JHM901.1, 2008.

1203

1204 Elder, K., Michaelsen, J., and Dozier, J.: Small basin modeling of snow water
1205 equivalence using binary regression tree methods, *IAHS Publ.* 228, 129–139, 1995.

1206

1207 Erickson, T. A., Williams, M.W., and Winstral, A.: Persistence of topographic controls
1208 on the spatial distribution of snow in rugged mountain terrain, Colorado, United States,
1209 *Water Res. Res.*, 41, W04014, doi:10.129/2003WR002973, 2005.

1210

1211 [Escher-Vetter, H., Kuhn, M., and Weber, M.: Four decades of winter mass balance of](#)
1212 [Vernagtferner and Hintereisferner, Austria: methodology and results, *Ann. Glaciol.*,](#)
1213 [50\(50\), 2009.](#)

1214 [Fausto, R.S., and 11 others.: A Snow Density Dataset for Improving Surface Boundary](#)
1215 [Conditions in Greenland Ice Sheet Firn Modeling, *Front. Earth Sci.*, 6\(51\),](#)
1216 [doi:10.3389/feart.2018.00051, 2018.](#)

1217 Fitzpatrick, N., Radić, V., and Menounos, B.: Surface energy balance closure and
1218 turbulent flux parameterization on a mid-latitude mountain glacier, Purcell Mountains,
1219 Canada, *Front. Earth Sci.*, 5(67), doi:10.3389/feart.2017.00067, 2017.

1220 Grünewald, T., and Lehning, M.: Altitudinal dependency of snow amounts in two alpine
1221 catchments: Can catchment-wide snow amounts be estimated via single snow or
1222 precipitation stations?, *Ann. Glaciol.*, 52(58), 153–158, 2011.

1223 Helfricht, K., Schöber, J., Schneider, K., Sailer, R., and Kuhn, M.: Interannual
1224 persistence of the seasonal snow cover in a glacierized catchment, *J. Glaciol.*, 60(223),
1225 doi:10.3189/2014JoG13J197, 2014.

1226

1227 Hock, R.: Glacier melt: a review of processes and their modeling, *Prog. Phys. Geog.*, 29,
1228 362–391, doi:10.1191/0309133305pp453ra, 2005.

1229

1230 Hock, R., Hutchings, J. K., and Lehning, M.: Grand challenges in cryospheric sciences:
1231 toward better predictability of glaciers, snow and sea ice, *Front. Earth Sci.*, 5(64),
1232 doi:10.3389/feart.2017.00064, 2017.

1233

1234 Hodgkins, R., Cooper, R., Wadham, J., and Tranter, M.: Interannual variability in the
1235 spatial distribution of winter accumulation at a high-Arctic glacier (Finsterwalderbreen,
1236 Svalbard), and its relationship with topography, *Ann. Glaciol.*, 42, 243–248, 2005.

1237

1238 Huss, M. and Hock, R.: A new model for global glacier change and sea-level rise, *Front.*
1239 *Earth Sci.*, 3, doi:10.3389/feart.2015.00054, 2015.

1240 Kaser, G., Großhauser, M., and Marzeion, B.: Contribution potential of glaciers to water
1241 availability in different climate regimes, *Proc. Natl. Acad. Sci.*, 107, 20,223–20,227,
1242 doi:10.1073/pnas.1008162107, 2010.

1243

1244 Klos, P. Z., Link, T. E., and Abatzoglou, J. T.: Extent of the rain-snow transition zone in
1245 the western U.S. under historic and projected climate, *Geophys. Res. Lett.*, 41, 4560–
1246 4568, doi: 10.1002/2014GL060500, 2014.

1247

1248 Knowles, N., Dettinger, M. D., and Cayan, D. R.: Trends in snowfall versus rainfall in
1249 the Western United States, *J. Climate*, 19, 4545–4559, 2006.

1250
1251 Kovacs, A., Gow, A. J., and Morey, R. M.: The in-situ dielectric constant of polar firm
1252 revisited, *Cold Reg. Sci. Tech.*, 23, 245–256, 1995.
1253
1254 Kuhn, M.: The mass balance of very small glaciers, *Z. Gletscherkd. Glazialgeol.*, 31(1–
1255 2), 171–179, 1995.
1256
1257 Lehning, M., Grünewald, T., and Schirmer, M.: Mountain snow distribution governed by
1258 altitudinal gradient and terrain roughness, *Geophys. Res. Lett.*, 38, L19504,
1259 doi:10.1029/2011GL048927, 2011.
1260
1261 Li, L. and Pomeroy, J. W.: Estimates of threshold wind speeds for snow transport using
1262 meteorological data, *J. Applied Met.*, 36, 205-213, 1997.
1263
1264 Liston, G. E., and Elder, K.: A distributed snow-evolution modeling system
1265 (SnowModel), *J. Hydromet.*, 7, 1259-1276, 2006.
1266
1267 Littel, J. S., McAfee, S. A., and Hayward, G. D.: Alaska snowpack response to climate
1268 change: statewide snowfall equivalent and snowpack water scenarios, *Water*, 10 (5), doi:
1269 10.3390/w10050668, 2018.
1270
1271 [Kjøllmoen, B. \(ed\), Andreassen L.M., Elvehøy, H., Jackson, M., and Melvold, J:](#)
1272 [Glaciological investigations in Norway 2016, NVE Rapport 76 2017, 108 pp, 2017.](#)
1273
1274 Marks, D., Domingo, J., Susong, D., Link, T., and Garen, D.: A spatially distributed
1275 energy balance snowmelt model for application in mountain basins, *Hydrol. Processes*,
1276 13, 1935–1959, 1999.
1277
1278 Machguth, H., Eisen, O., Paul, F., and Hoelzle, M.: Strong spatial variability of snow
1279 accumulation observed with helicopter-borne GPR on two adjacent Alpine glaciers,
1280 *Geophys. Res. Lett.*, 33, L13503, doi:10.1029/2006GL026576, 2006.

1281
1282 March, R. S., and Trabant, D. C.: Mass balance, meteorological, ice motion, surface
1283 altitude, and runoff data at Gulkana Glacier, Alaska, 1992 balance year, Water-Resources
1284 Investigations Report, 95-4277, 1996.
1285
1286 McAfee, S., Walsh, J., and Rupp, T. S.: Statistically downscaled projections of snow/rain
1287 partitioning for Alaska, *Hydrol. Process.*, 28(12), 3930–3946, doi:10.1002/hyp.9934,
1288 2013.
1289
1290 McGrath, D., Sass, L., O’Neel, S., Arendt, A., Wolken, G., Gusmeroli, A., Kienholz, C.,
1291 and McNeil, C.: End-of-winter snow depth variability on glaciers in Alaska, *J. Geophys.*
1292 *Res. Earth Surf.*, 120, 1530–1550, doi:10.1002/2015JF003539, 2015.
1293
1294 McGrath, D., Sass, L., O’Neel, S., Arendt, A. and Kienholz, C.: Hypsometric control on
1295 glacier mass balance sensitivity in Alaska and northwest Canada, *Earth’s Future*, 5, 324–
1296 336, doi:10.1002/2016EF000479, 2017.
1297
1298 Meromy, L., Molotch, N. P., Link, T. E., Fassnacht, S. R., and Rice, R.: Subgrid
1299 variability of snow water equivalent at operational snow stations in the western USA,
1300 *Hydro. Proc.*, 27, 2383–2400, doi:10.1002/hyp.9355, 2013.
1301
1302 Molotch, N. P., Colee, M. T., Bales, R. C. and Dozier, J.: Estimating the spatial
1303 distribution of snow water equivalent in an alpine basin using binary regression tree
1304 models: the impact of digital elevation data and independent variable selection, *Hydrol.*
1305 *Proc.*, 19, 1459–1479, doi:10.1002/hyp.5586, 2005.
1306
1307 Nolan, M., Larsen, C., and Sturm, M.: Mapping snow depth from manned aircraft on
1308 landscape scales at centimeter resolution using structure-from-motion photogrammetry,
1309 *The Cryosphere*, 9, 1445–1463, doi:10.5194/tc-9-1445-2015, 2015.
1310

1311 Noh, M. J. and Howat, I. M.: Automated stereo-photogrammetric DEM generation at
1312 high latitudes: Surface Extraction with TIN-based Search-space Minimization (SETSM)
1313 validation and demonstration over glaciated regions, *GIScience & Remote*
1314 *Sensing*, 52(2), 198-217, doi:10.1080/15481603.2015.1008621, 2015.
1315

1316 O’Neel, S., Hood, E., Arendt, A., and Sass, L.: Assessing streamflow sensitivity to
1317 variations in glacier mass balance, *Climatic Change*, 123(2), 329–341,
1318 doi:10.1007/s10584-013-1042-7, 2014.
1319

1320 O’Neel, S., Fagre, D. B., Baker, E. H., Sass, L. C., McNeil, C. J., Peitzsch, E. H.,
1321 McGrath, D. and Florentine, C. E.: Glacier-Wide Mass Balance and Input Data: USGS
1322 Benchmark Glaciers, 1966-2016 (ver. 2.1, May 2018), U.S. Geological Survey data
1323 release, <https://doi.org/10.5066/F7HD7SRE>, 2018.
1324

1325 Painter, T., Berisford, D., Boardman, J., Bormann, K., Deems, J., Gehrke, F., Hedrick,
1326 A., Joyce, M., Laidlaw, R., Marks, D., Mattmann, C., McGurk, B., Ramirez, P.,
1327 Richardson, M., Skiles, S.M., Seidel, F., and Winstral, A.: The Airborne Snow
1328 Observatory: fusion of scanning lidar, imaging spectrometer, and physically-based
1329 modeling for mapping snow water equivalent and snow albedo, *Remote Sens. Environ.*,
1330 184, 139–152, doi:10.1016/j.rse.2016.06.018, 2016.
1331

1332 [Pelto, M.: Utility of late summer transient snowline migration rate on Taku Glacier,](#)
1333 [Alaska, *The Cryosphere*, 5, 1127–1133, doi:10.5194/tc-5-1127-2011, 2011.](#)

1334

1335 [Pelto, M., Kavanaugh, J., and McNeil, C.: Juneau Icefield Mass Balance Program](#)
1336 [1946–2011, *Earth Syst. Sci. Data*, 5, 319-330, \[https://doi.org/10.5194/essd-5-319-\]\(https://doi.org/10.5194/essd-5-319-2013\)](#)
1337 [2013, 2013.](#)

1338

1339 Pérez-Ruiz, M., Carballido, J., and Agüera, J.: Assessing GNSS correction signals for
1340 assisted guidance systems in agricultural vehicles, *Precision Agric.*, 12, 639–652,
1341 doi:10.1007/s11119-010-9211-4, 2011.

1342
1343 Pfeffer, W. T., and Bretherton, C.: The effect of crevasses on the solar heating of a
1344 glacier surface, *IAHS Publ.*, 170, 191–205, 1987.
1345
1346 Pfeffer, W. T., et al.: The Randolph Glacier Inventory: A globally complete inventory of
1347 glaciers, *J. Glaciol.*, 60(221), 537–552, doi:10.3189/2014JoG13J176, 2014.
1348
1349 Schirmer, M., Wirz, V., Clifton, A., and Lehning, M.: Persistence in intra-annual snow
1350 depth distribution: 1. Measurements and topographic control, *Water Resour. Res.*, 47,
1351 W09516, doi:10.1029/2010WR009426, 2011.
1352
1353 Sold, L., Huss, M., Hoelzle, M., Andereggen, H., Joerg, P., and Zemp, M.:
1354 Methodological approaches to infer end-of-winter snow distribution on alpine glaciers, *J.*
1355 *Glaciol.*, 59(218), 1047–1059, doi:10.3189/2013JoG13J015, 2013.
1356
1357 Sold, L., Huss, M., Machguth, H., Joerg, P. C., Vieli, G. L., Linsbauer, A., Salzmann, N.,
1358 Zemp, M. and Hoelzle, M.: Mass balance re-analysis of Findelengletscher, Switzerland;
1359 Benefits of extensive snow accumulation measurements, *Front. Earth Sci.*, 4(18),
1360 doi:10.3389/feart.2016.00018, 2016.
1361
1362 Sturm, M. and Wagner, A. M.: Using repeated patterns in snow distribution modeling:
1363 An Arctic example, *Water Res. Res.*, 46 (12), doi:10.1029.2010WR009434, 2010.
1364
1365 Van Beusekom, A. E., O’Neel, S., March, R. S., Sass, L., and Cox, L. H.: Re-analysis of
1366 Alaskan Benchmark Glacier mass balance data using the index method, U.S. Geological
1367 Survey Scientific Investigations Report 2010–5247, 16 p., 2010.
1368

1369 [Vincent, C., Fischer, A., Mayer, C., Bauder, A., Galos, S.P., Funk, M., Thibert, E., Six,](#)
1370 [D., Braun, L., and Huss, M.: Common climatic signal from glaciers in the European Alps](#)
1371 [over the last 50 years, *Geophys. Res. Lett.*, 44, 1376–1383, doi:10.1002/2016GL072094,](#)
1372 [2017.](#)

1373
1374 Winstral, A., Elder, K., and Davis, R. E.: Spatial snow modeling of wind-redistributed
1375 snow using terrain-based parameters, *J. Hydrometeo.*, 3, 524–538, 2002.

1376
1377 Winstral, A., Marks, D. and Gurney, R.: Simulating wind-affected snow accumulations at
1378 catchment to basin scales, *Adv. Water Res.*, 55, 64–79,
1379 doi:10.1016/j.advwatres.2012.08.011, 2013.

1380
1381 Winstral, A. and Marks, D.: Long-term snow distribution observations in a mountain
1382 catchment: Assessing variability, time stability, and the representativeness of an index
1383 site, *Water Res. Res.*, 50, 293–305, doi:1002/2012WR013038, 2014.

1384
1385 Woo, M.-K., and Marsh, P.: Analysis of error in the determination of snow storage for
1386 small high Arctic basins, *J. Appl. Meteorol.*, 17, 1537–1541, 1978.

1387
1388 Yelf, R. and Yelf, D.: Where is true time zero?, *Electro. Phenom.*, 7(1), 158–163, 2006.

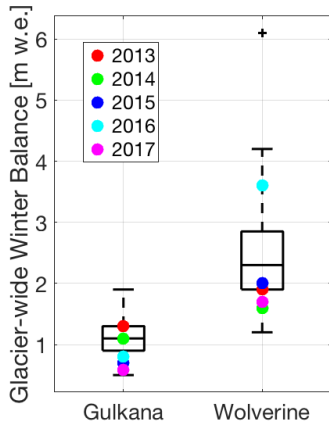
1389
1390
1391
1392
1393
1394
1395
1396
1397
1398
1399
1400
1401
1402
1403

1404 Figure 1. Map of southern Alaska with study glaciers marked by red outline. All glaciers
1405 in the region are shown in white (Pfeffer et al., 2014).



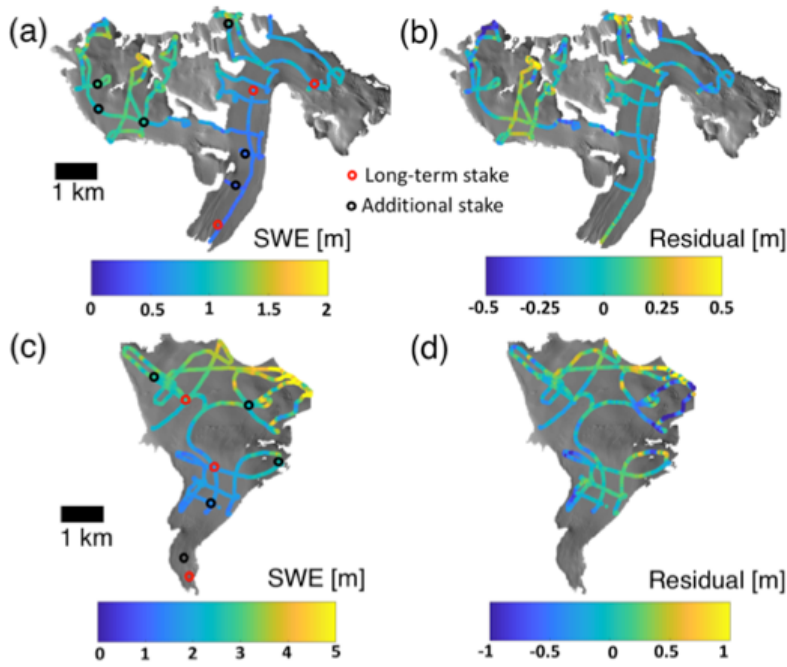
1406
1407
1408
1409
1410

1411 Figure 2. Boxplots of glacier-wide winter balance for Gulkana and Wolverine glaciers
1412 between 1966 and 2017. Years corresponding to GPR surveys are shown with colored
1413 markers. These values have not been adjusted by the geodetic calibration (see O'Neel et
1414 al., 2014).

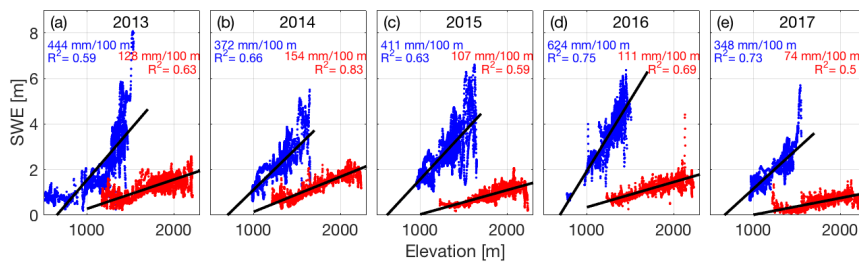


1415
1416
1417
1418

1419 Figure 3. GPR surveys from 2015 at Gulkana (a) and Wolverine (c) glaciers and MVR
 1420 model residuals (b, d).

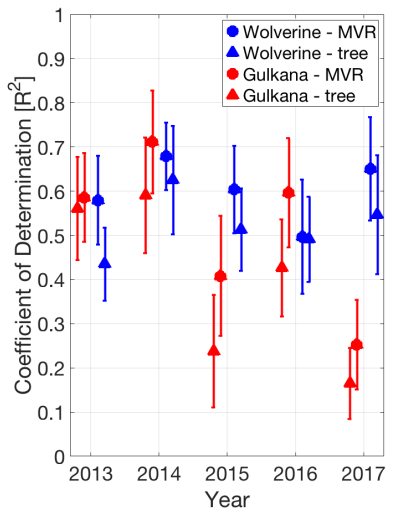


1421
 1422
 1423
 1424 Figure 4. SWE from GPR surveys as a function of elevation, along with least squares
 1425 regression slope and coefficient of determination for each year of the study period.
 1426 Wolverine is plotted in blue, Gulkana in red.



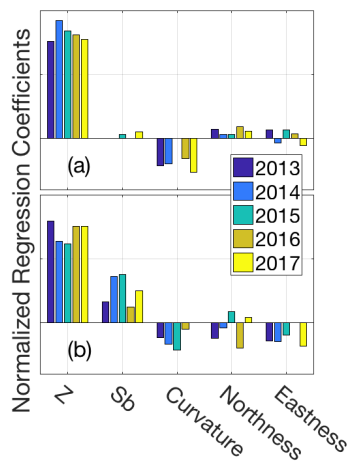
1427
 1428

1429 Figure 5. Median and standard deviation (error bars) of coefficient of determination
 1430 (from 100 model runs) for both extrapolation approaches (circles are MVR, triangles are
 1431 regression tree) developed on training datasets and applied to test datasets. Symbols and
 1432 error bars are offset from year for clarity.



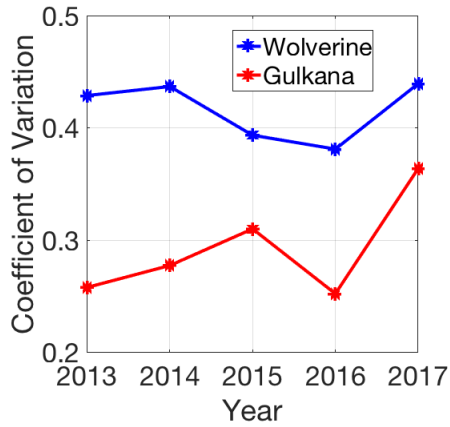
1450

1451 Figure 6. Terrain parameter beta coefficients for (a) Gulkana and (b) Wolverine for
 1452 multivariable linear regression for each year of the study interval.



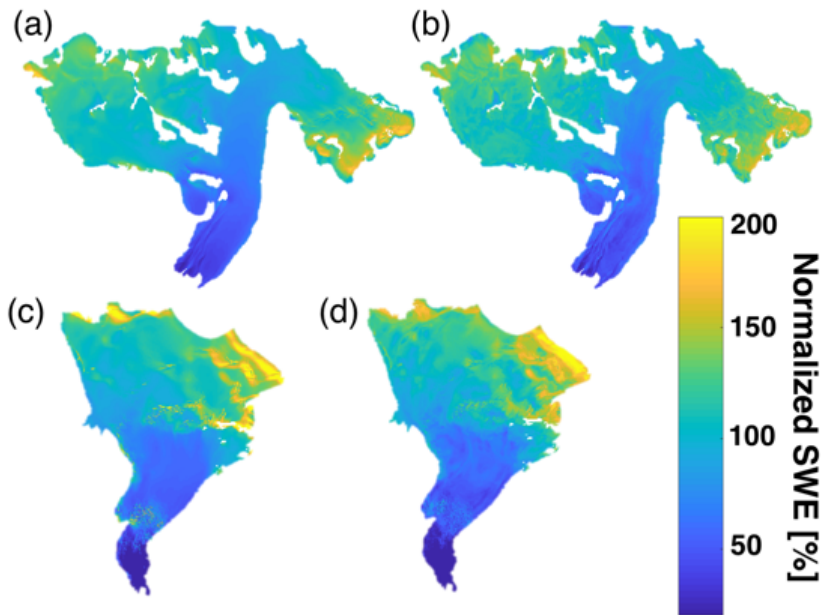
1453

1454 Figure 7. Spatial variability in snow accumulation across the glacier quantified by the
1455 coefficient of variation (standard deviation/mean) for each glacier across the five-year
1456 interval based on MVR model output.
1457



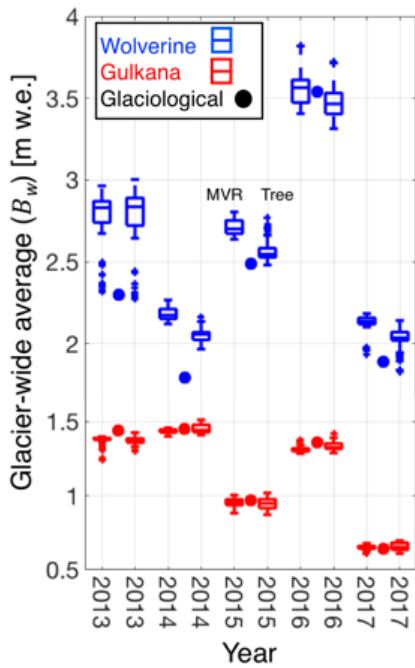
1458
1459
1460
1461

Figure 8. Five-year mean of normalized distributed SWE for Gulkana (a,b) and Wolverine (c,d) for multivariable regression (a,c) and regression tree (b,d).



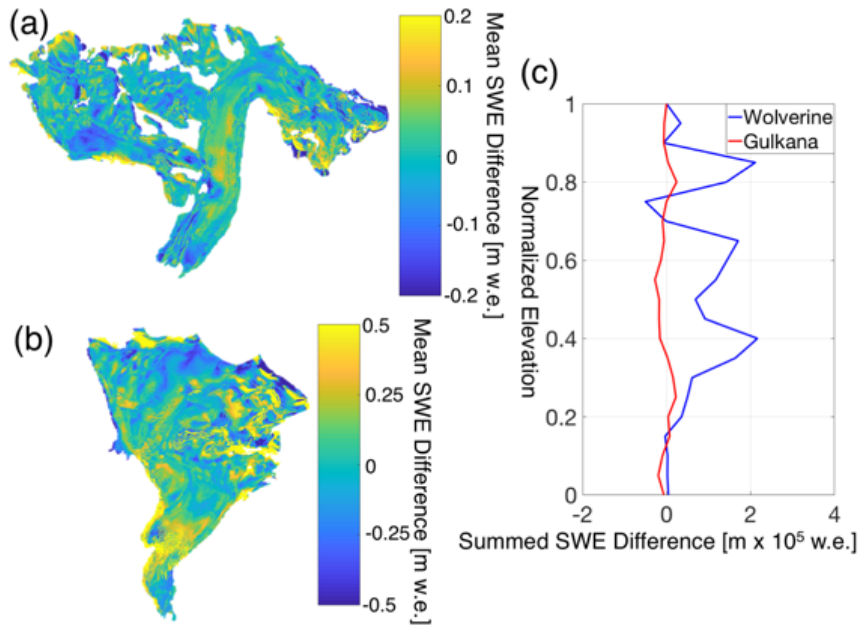
1462

1463 Figure 9. Comparing statistical models for GPR-derived glacier-wide winter balances for
 1464 both Wolverine (blue) and Gulkana (red) glaciers. For each year and each glacier, two
 1465 boxplots are shown. The first shows multivariable regression model (MVR) output and
 1466 the second shows regression tree output (tree). The B_w estimate from the glaciological
 1467 profile method is shown for each year and glacier as the filled circle.
 1468



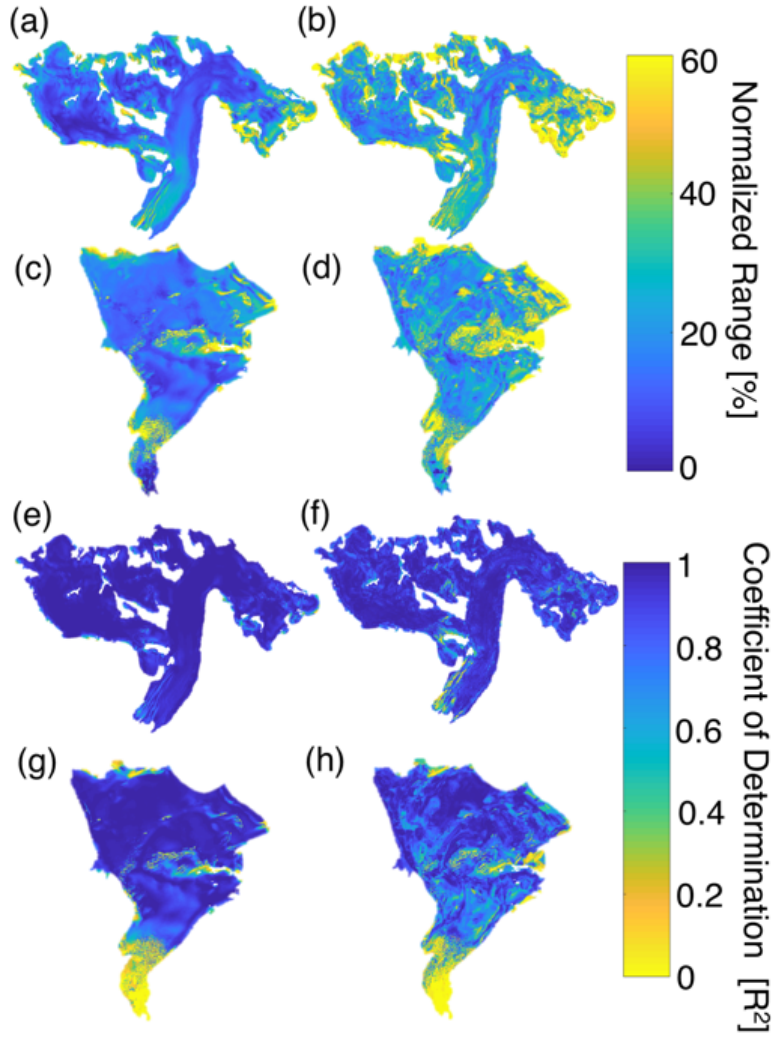
1469
 1470
 1471
 1472
 1473
 1474
 1475
 1476
 1477
 1478
 1479

1480 Figure 10. SWE differences between statistical models for Gulkana (a) and Wolverine
1481 (b) calculated by differencing the regression tree five-year mean SWE from the
1482 multivariable regression (MVR) five-year mean SWE. Yellow colors indicate regions
1483 where MVR yields more SWE than decision tree and blue colors indicate the opposite.
1484 Note different magnitude colorbar scales. c) Summed SWE difference between methods
1485 in bins of 0.05 normalized elevation values.



1486
1487
1488
1489
1490
1491
1492
1493
1494
1495
1496
1497
1498
1499

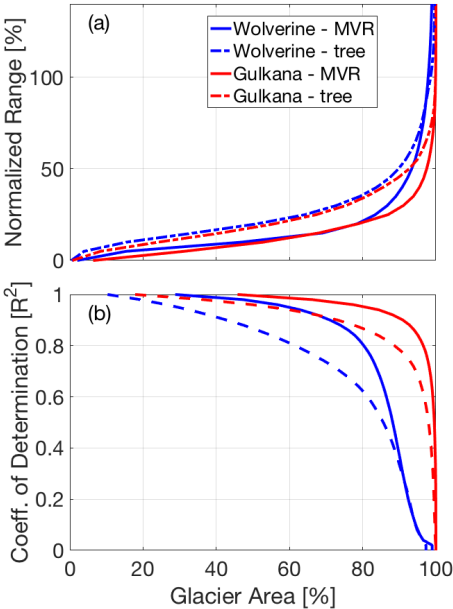
1500 Figure 11. Interannual variability of the SWE accumulation field from 2013–2017,
1501 quantified via normalized range (a-d) and R^2 (e-h) approach for median distributed fields
1502 from the multivariable regression (left column) and regression tree (right column)
1503 statistical models.



1504
1505

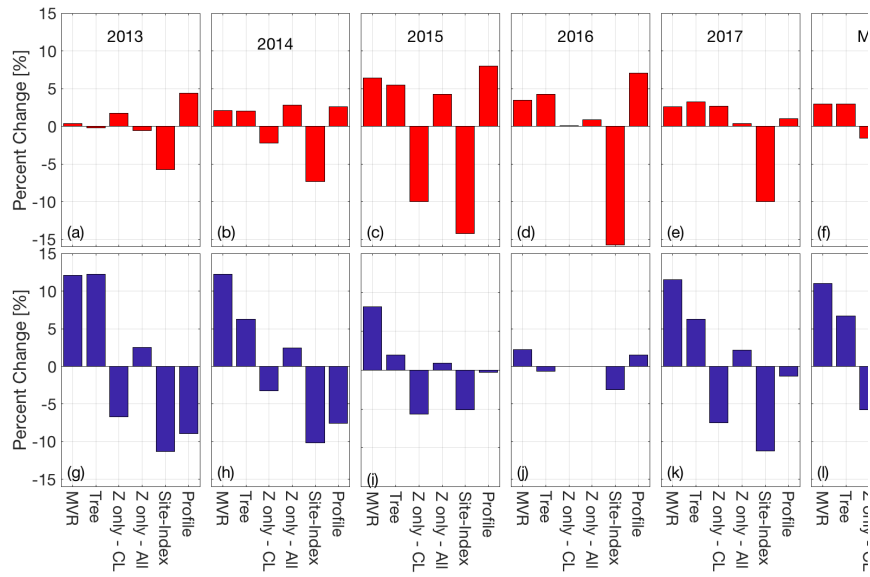
Deleted: r^2

1506 Figure 12. Interannual variability of the SWE accumulation pattern as a function of
1507 cumulative glacier area, shown as (a) normalized range and (b) and R^2 . Solid lines are for
1508 multivariable regression (MVR) and dashed lines are regression tree.
1509



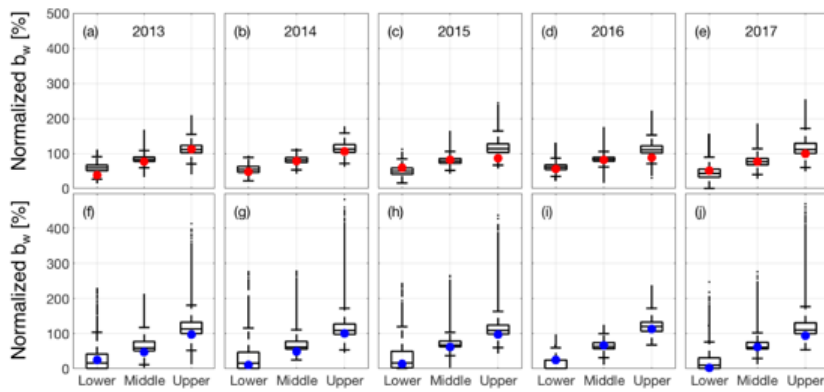
1510
1511
1512
1513
1514
1515
1516
1517
1518
1519
1520
1521
1522
1523
1524

1526 Figure 13. Percent deviation for each estimate from the six-method mean of B_{yr} .
 1527 Individual years for Gulkana Glacier are shown in panels a-e with the five-year mean
 1528 shown in f. Individual years for Wolverine Glacier are shown in panels g-k, with the five-
 1529 year mean shown in l.



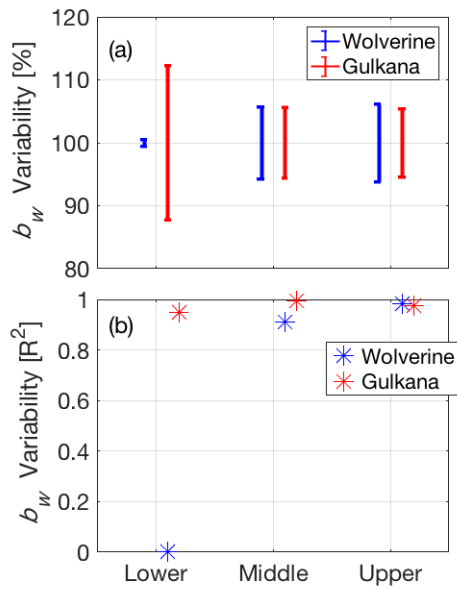
1530
 1531
 1532
 1533
 1534
 1535
 1536
 1537
 1538
 1539
 1540
 1541
 1542
 1543
 1544
 1545

1546 Figure 14. Spatial variability in snow accumulation for individual years (2013-2017) by
 1547 elevation (lower, middle, upper) compared to stake measurements. Box plot of all
 1548 distributed SWE values (from multivariable regression) for each index zone of the glacier
 1549 for Gulkana (a-e) and Wolverine (f-j) for 2013-2017. The filled circles are the respective
 1550 stake observation for that index zone. SWE is expressed as a percentage of the glacier-
 1551 wide average, B_w , for that year and glacier.



1552
 1553
 1554
 1555
 1556
 1557
 1558
 1559
 1560
 1561
 1562
 1563
 1564
 1565
 1566
 1567
 1568
 1569
 1570
 1571

1572 Figure 15. Interannual variability in the spatial pattern of snow accumulation at long-term
 1573 mass balance stake locations for Wolverine and Gulkana glaciers using a) normalized b_w
 1574 range and b) coefficient of determination (from Figure 11; MVR model).
 1575



1576
 1577
 1578
 1579
 1580
 1581
 1582
 1583
 1584
 1585
 1586
 1587